Original Research Article
TRA.12465
doi: 10.1111/TRA.12XXX
Society number TRA-16-0545
NIH funded NO
Manuscript received 31 July 2016
Revised and accepted 13 December 2016
Sent to press 13 December 2016
Color figures: Figures 1, 2, 3, 4, 5, 6, 7, 8, 9,11
Halftone figures: Figure 10
Supplemental figures (legends only to be included in typeset manuscript): 5 figures
Synopsis included YES
Abstract figure included YES
Editorial process file included YES

Amyloid precursor protein traffics from the Golgi directly to early endosomes in an Arl5b and AP4 dependent pathway

Wei Hong Toh[*], Jing Zhi A. Tan[*], Khalisah L. Zulkefli[*], Fiona J. Houghton[*] and Paul A. Gleeson[*]

[*]The Department of Biochemistry and Molecular Biology and Bio21 Molecular Science and Biotechnology Institute, The University of Melbourne, Victoria 3010

Running Title: Arl5b and AP4 mediate post-Golgi APP transport

Corresponding author: Prof. Paul Gleeson, Department of Biochemistry and Molecular Biology and Bio21 Molecular Science and Biotechnology Institute, The University of Melbourne, Victoria 3010, Australia
Phone 61-3-8344-2354: Fax 61-3-9348-1428, E-mail: pgleeson@unimelb.edu.au

Key words: Anterograde transport, Arl5b, AP4, amyloid precursor protein, amyloid ² peptide, early endosomes, *trans*-Golgi network

Synopsis: The membrane trafficking of newly synthesised amyloid precursor protein (APP) from the Golgi to the endolysosomal system is not well defined, yet is critical for understanding the processing of APP. We demonstrate that the small G protein Arl5b recruits the adaptor complex AP4 to the *trans*-Golgi network (TGN) which regulates APP transport from the TGN directly to early endosomes. Our findings also show that the post-Golgi trafficking of newly synthesised APP is relevant for the regulation of amyloid ² production.

Abbreviations: A², eta-amyloid peptide; BACE1, beta site APP-cleaving enzyme: APP, amyloid precursor protein; TGN, trans-Golgi network; TfR, transferrin receptor

Abstract

The intracellular trafficking and proteolytic processing of the membrane-bound amyloid precursor protein (APP) are co-ordinated events leading to the generation of pathogenic amyloid-beta (Aβ) peptides. The membrane transport of newly synthesised APP from the Golgi to the endolysosomal system is not well defined, yet is likely to be critical for regulating its processing by β-secretase (BACE1) and γ-secretase. Here we show that the majority of newly synthesised APP is transported from the *trans*-Golgi network (TGN) directly to early endosomes and then subsequently to the late endosomes/lysosomes with very little transported to the cell surface. We show that Arl5b, a small G protein localized to the TGN, and AP4 are essential for the post-Golgi transport of APP to early endosomes. Arl5b is physically associated with AP4 and is required for the recruitment of AP4, but not AP1, to the TGN. Depletion of either Arl5b or

AP4 results in the accumulation of APP, but not BACE1, in the Golgi, and an increase in APP processing and Aβ secretion. These findings demonstrate that APP is diverted from BACE1 at the TGN for direct transport to early endosomes and that the TGN represents a site for APP processing with the subsequent secretion of A².

Introduction

Extracellular amyloid plaque deposits composed of amyloid-beta (Aβ) peptides are a pathological hallmark of Alzheimer's disease (AD). Aβ peptides are released from the amyloid precursor protein (APP) by the sequential cleavage by ²-secretase (BACE1) and ³-secretase in a process termed amyloidogenic APP processing. In an alternative non-amyloidogenic pathway, APP is cleaved by ±-secretase and the subsequent cleavage by ³-secretase precludes the formation of the A² peptide. APP processing is likely to occur in multiple compartments in the cell as the membrane-bound secretases involved in the processing of APP can traffic through both secretory and endocytic pathways. The non-amyloidogenic processing of APP is generally considered to occur predominantly on the plasma membrane due to high abundance of ±-secretase at this location [1], although there are reports that ±-secretase cleavage of APP can also occur in the secretory pathway [2]. In contrast, amyloidogenic processing of APP occurs in intracellular compartments. There is substantial evidence that A² can be generated in the endosomal system [3], considered to arise from the internalisation of APP from the PM, and there is general consensus that under normal conditions the early endosome is a major site of APP processing by BACE1 [4-7]. Although less well characterised there are also several reports which have indicated that A² can be generated in the secretory pathway [8-10], in particular the TGN [11-13].

APP is synthesised in the ER, and then transported to the Golgi where it is glycosylated and the mature glycoprotein then exits the Golgi at the TGN [14]. It has been widely assumed that APP is transported along the anterograde transport pathway from the TGN to the PM, however, the transport route of APP from the TGN is poorly defined. The TGN is a major sorting compartment of the secretory pathway [15,16] where membrane cargos are packaged into different membrane carriers for post-Golgi transport. The recruitment of many cargos into transport carriers at the TGN is mediated by adaptor protein complexes (AP) which bind to sorting motifs on the cytoplasmic tails of proteins. The binding of AP complexes to the TGN is regulated by small G proteins of the ADP-ribosylation factor (Arf) family [17]. Membrane cargo destined for the plasma membrane (PM) are transported from the TGN either directly to the PM or by an indirect route via endosomes, usually the recycling endosomes [18,19]. Cargo from the TGN can also be trafficked to the endosomes, such as the mannose-6-phosphate receptor which is transported by AP1 to the late endosomes [20,21].

The cytoplasmic tail of APP is 47 residues and contains three sorting motifs [22-24], each with the potential to mediate APP trafficking at one or more intracellular sites [25]. Two adaptors have been reported to bind to APP motifs at the TGN. Interestingly, the μ subunit of the TGN-localised adaptor protein complex, AP4, has been shown to bind to the YKFFE motif in the cytoplasmic tail of APP in *in vitro* studies [10]. Depletion of AP4μ resulted in a shift in the steady state intracellular distribution of APP and an accumulation of APP in the TGN. These findings by the Bonifacino lab suggests that AP4 is involved in regulating the post-Golgi transport of APP from the TGN [10]. In an earlier study by the same group the small G protein, Arf1 was shown to interact with AP4 by yeast two hybrid assays [26]. However, whether Arf1 is required for the recruitment of AP4 to TGN membranes and the anterograde transport of APP *in vivo* remains unclear. The Mint/X11 family of adaptor proteins has also been shown to interact with the GYENPTY motif on APP [27,28]. In particular Mint3 localizes to the TGN and influences the exit of APP from the Golgi in transiently transfected cultured cells.

Knowledge of the intracellular trafficking itinerary of APP is important to better appreciate how the intracellular location of APP influences its exposure to β- and γ-secretases and thereby regulated the rate of processing and generation of A². Here we demonstrate that newly synthesised APP is trafficked directly from the TGN to the early endosomes, with very little transported to the cell surface. Moreover we have discovered that post-Golgi transport of APP is regulated by an Arf-like small G protein, Arl5b and the adaptor protein complex, AP4. Disruption of Arl5b/AP4 function increases A² production demonstrating that the TGN is an important intracellular site for APP processing. Our findings highlight the importance of the intracellular trafficking of APP and demonstrate that the post-Golgi trafficking of newly synthesised APP is relevant for the regulation of A² production.

Results

Newly synthesised APP traffics from TGN to early endosomes

To investigate the membrane transport of APP we generated a stable HeLa cell line expressing APP_{695wt} as endogenous APP in HeLa cells is very low (Fig. S1D). At steady state the majority of the APP was associated with early endosomes and late endosomes, with very little detected in either recycling endosomes or the cell surface (Fig. S1A, B, C and Fig. 1C, D). Dual staining of HeLa cells stably expressing APP_{695wt} with antibodies specific for both the N-terminal domain and C-terminal tail of APP demonstrated a high level of overlap demonstrating that the APP product detected in the fixed and permeabilized cells was intact membrane-bound APP and not a cleaved product of APP. The level of APP_{695wt} in the stable cell line was 12.9 fold higher than in wild-type HeLa cells (Fig. S1D). This represents a modest increase of

APP level compared with transient expression of APP which can be >30 fold over endogenous level (data not shown).

To investigate the anterograde transport of APP, newly synthesised APP was monitored in HeLa cells stably expressing APP_{695wt} following treatment with cycloheximide (CHX) to allow the turnover of the existing APP pool (Fig. 1A). CHX interferes with translational elongation and the inhibition by CHX can be rapidly reversed by removing the inhibitor from the culture medium. Three hours of CHX treatment was a sufficient period for the turnover of the majority of cellular APP (data not shown), kinetics consistent with the trafficking of mature APP along the endo/lysosomal pathway [29]. A longer period of 4 h was chosen in the subsequent experiments to ensure that the existing pool of APP was fully depleted. After 4 h CHX treatment, the drug was removed from the culture medium and protein synthesis allowed to resume. Cells were fixed at different time points over a period of 2 h (Fig. 1A) and the intracellular location of newly synthesised APP in intracellular compartments was tracked using appropriate markers.

In untreated cells, APP localized predominantly in endosomal compartments as shown by the co-localization with the early endosome and late endosome markers, EEA1 and Rab7 respectively, and there was little overlap between APP with the TGN marker, GCC88 (Fig. 1B). After a 4 h treatment with CHX, very little APP staining was detected (Fig. 1B). By 1 h after CHX washout (recovery) APP was observed which represents newly synthesised material. At this time point >60% of the newly synthesised APP co-localized with the Golgi/TGN marker GCC88 (Fig. 1B, C), indicating that the majority of the newly synthesised APP had exited the ER and arrived at the Golgi apparatus. At this time point there was also little overlap (< 10 %) with the endosomal markers, EEA1 and Rab7, indicating that the majority of APP had not exited the TGN and trafficked to other compartments. However by 1.5 h CHX washout a shift in the APP distribution was observed and 40% of APP overlapped with EEA1, indicating that the newly synthesised APP had exited the TGN and trafficked to early endosomes (Fig. 1B, C). At this 1.5 h time point there was a minimal overlap with Rab7 (<10 %), indicating that APP traffics directly from the TGN to the early endosomes rather than the late endosomes (Fig. 1B,C). After a 2 h chase period the level of APP in the TGN decreased to ~10% of the total cell distribution, a percentage which is similar to steady state conditions, and there was increased localisation in late endosomes (30-40%) (Fig. 1B,C), indicating that the wave of newly synthesised APP has exited the early endosomes and trafficked to later compartments in the endolysosomal pathway.

A number of new synthesised cargos traffic to the PM via the recycling endosomes [15]. To investigate if newly synthesised APP also traffics to the recycling endosomes from the TGN, the localisation of APP with the recycling endosome marker, Rab11, was examined. In untreated cells, there was minimal overlap of APP with Rab11 (< 10%) (Fig. 1D). Very little overlap between APP and Rab11 was also observed over an extended 7 hour chase period following CHX washout (Fig. 1D, Fig. S2), indicating that very little, if any, newly synthesised APP is transported from the Golgi to the recycling endosomes.

Taken together, these results show that newly synthesised APP exits the TGN and is transported to endosomes. Moreover, the kinetics of APP trafficking strongly suggests that APP traffics directly to the early endosomes.

Newly synthesised APP is transported by a direct route to the endosomal pathway

The findings above suggest a direct transport of APP from the TGN to the early endosomes. Subsequent trafficking of APP from the early endosomes to the late endosomes could either be a direct transport step or an indirect pathway initially to the plasma membrane followed by rapid internalisation. To determine whether newly synthesised APP was transported to the PM, HeLa cells stably expressing APP_{695wt} were treated with CHX for 4 h as previously, the drug was removed for 1 h 15 min to allow newly synthesised APP to accumulate in the Golgi and early endosomes and then Pitstop 2, an inhibitor of clathrin which selectively blocks clathrin mediated endocytosis [30], was added to block AP2/clathrin dependent endocytosis from the PM (Fig. 2A, B). As cells begin to detach after 60 min treatment with Pitstop 2 the incubation with this inhibitor was restricted to 45 min, which represents the window of the chase when the wave of newly synthesised APP is transported along the endolysosomal pathway. If APP was transported via the PM, then it would accumulate at the PM in the presence of Pitstop 2. However, the levels of APP in the early endosome and the late endosome were unaffected by Pitstop 2 (Fig. 2C) and the distribution between the early and late endosomes was very similar to the previous experiment (Fig. 1), indicating that the bulk of the APP was transported to late endosomes directly from the early endosomes. Very little APP was detected at the cell surface after a 45 min Pitstop 2 treatment, whereas Pitstop 2 resulted in the accumulation of the transferrin receptor at the cell surface (Fig. 2D and Fig S3) indicating that clathrin-mediated endocytosis had indeed been blocked by this inhibitor.

APP distribution is not altered by Arf1 depletion

The TGN adaptor protein complex, AP4, has been shown to interact with the YKFFE sorting motif on the cytoplasmic tail of APP and to regulate the transport of APP from the TGN [10]. Adaptor protein complexes are recruited to the TGN membranes by small G proteins of the Arf/Arl family. In a previous study from the same group, they showed that the small G protein Arf1 is able to interact with AP4, based on a yeast 2-hybrid assay, and these authors proposed that the recruitment of AP4 to the TGN is regulated by Arf1 [26]. However, whether Arf1 regulates APP anterograde transport from the Golgi is unknown. To examine if Arf1 is involved in AP4-mediated APP trafficking, Arf1 was depleted in HeLa cells stably expressing APP_{695wt} using two siRNA target sequences to Arf1, and the steady state distribution of APP then analysed. If Arf1 is required for the post-Golgi export of

APP, APP would be expected to accumulate in the TGN. Both siRNA target sequences were successful in depleting Arf1 protein levels by >90% (Fig. 3A), however depletion of Arf1 by either Arf1 siRNA showed no change in the distribution of APP (Fig. 3B) compared with control siRNA treated cells. Quantitation revealed approximately 10% of APP co-localised with the TGN marker, GCC88, following Arf1 depletion (Fig. 3C, D), which is similar to untreated and control siRNA treated cells. It is possible that Arf1 is functionally redundant as both Arf1 and the closely related Arf4 need to be silenced to interfere with the recruitment of the TGN adaptor AP1 [31]. To provide a positive control for the loss of function of Arf1 we next depleted both Arf1 and Arf4 simultaneously and obtained a >90% depletion for Arf1 and 70% depletion for Arf4 (Fig. 3B). Depletion of both Arf1/Arf4 resulted in loss of AP1γ from the Golgi (Fig. 3E), as expected. However, only low levels of APP co-localised with the TGN marker in double knock down cells, as for the single knock down of Arf1 (Fig. 3D), findings which demonstrate that Arf1 is unlikely to be involved in regulating the post-Golgi trafficking of APP.

Depletion of the TGN localised Arl5b alters APP distribution

Since Arf1 is unlikely to regulate APP anterograde transport, we sought to identify a small G protein that could regulate post-Golgi APP transport. Work from our laboratory has demonstrated that Arl5b is located at the TGN and regulates transport between the endosome and TGN transport [32]. Given a potential role of Arl5b in TGN to endosome transport, we examined whether Arl5b might regulate the post-Golgi transport of APP. As antibodies are not available to detect endogenous Arl5b, we tested the efficiency of Arl5b depletion by assessing the decrease in the level of GFP in HeLa cells stably expressing Arl5b(Q70L)-GFP, a GFP fusion with the constitutive active form a Arl5b. Two independent Arl5b siRNA target sequences showed efficient depletion of GFP-Arl5b (>90%) as assessed by both immunoblotting and immunofluorescence for the GFP tag (Fig. 4A, B). Previous studies using qRT-PCR has shown that endogenous Arl5b is depleted using the same Arl5b siRNAs [32]. Hence silencing of GFP-Arl5b is also a read out for the silencing of endogenous Arl5b.

Depletion of Arl5b in HeLa cells stably expressing APP_{695wt} resulted in a dramatic change in distribution of APP with a shift to a juxtanuclear localization that overlapped extensively with the TGN marker GCC88 (Fig. 4C). Quantitation revealed that Arl5b depletion increased co-localization between APP and GCC88 from 10% in control siRNA treated cells to 20-30% in Arl5b treated cells (Fig. 4D). The Golgi localised APP represents intact membrane bound APP as dual staining with antibodies specific for both the N-terminal domain and C-terminal tail of APP demonstrated a high level of overlap in the fixed and permeabilized Arl5b depleted cells (Fig. S4). To exclude off target effects of the siRNAs we used an siRNA-1 resistant Arl5b-GFP mutant [32] and expressed this Arl5b mutant in siRNA treated APP_{695wt} expressing HeLa cells (Fig. 4E). Rescued cells were detected by GFP expression. APP did not accumulate in the Golgi in cells expressing the Arl5b rescue construct, confirming that the shift in APP distribution was due specifically to the depletion Arl5b. One complication with using full length APP is that the antibody to APP binds to the N-terminal region of APP which is released following BACE1 cleavage. Hence it is formally possible that detection of APP in the above experiment is due to cleaved extra-luminal product of APP that lacks the APP sorting signals located on the C-terminal cytoplasmic tail of APP. To define the intracellular distribution of APP molecule in the absence of cleavage, we used an CD8/APP construct containing the luminal and TM domains of CD8 fused to the cytoplasmic tail of APP, as described previously [33] [29]. Arl5b depletion also shifted the distribution of CD8/APP to the TGN with the level of co-localisation of CD8/APP and the TGN marker GCC88 similar to that observed for full length APP (Fig. 5A, B). Hence, collectively these data show that Arl5b may be involved in the post-Golgi transport of APP.

Previously work in our laboratory showed that Arl5b depletion did not affect the anterograde transport of E-cadherin, a membrane protein that utilizes the transport route to the PM via the recycling endosomes [32]. Hence Arl5b may regulate post-Golgi transport selectively to early/late endosomes. To assess whether Arl5b depletion impacted on post-Golgi export of other proteins from the TGN, the effects of Arl5b depletion on BACE1 distribution was also investigated. Arl5b depletion using either Arl5b-1 or Arl5b-2 siRNAs had no effect on BACE1 distribution (Fig. S5). These data indicates that the effect of Arl5b depletion is specific for the post-Golgi transport of APP. Moreover, the findings also imply that APP and BACE1 are segregated into distinct anterograde transport pathways from the TGN.

To investigate a potential relationship between Arl5b and AP4, we depleted the μ subunit of AP4 in HeLa cells stably expressing APP_{695wt} using two independent siRNAs target sequences to AP4μ to determine the impact of AP4 on APP post-Golgi trafficking (Fig. 6A). Depletion of any of the four subunits in the AP4 complex is likely to disrupt the assembly of AP4 complex and thus would disrupt its function and localization of AP4. As assessed by qRT-PCR, there was ~90% and ~60% efficiency in AP4μ depletion using AP4μ-1 siRNA and AP4μ-2 siRNA, respectively (Fig. 6A). Depletion of AP4μ resulted in a dramatic shift in APP distribution to the TGN (Fig. 6B), consistent with previous report from Burgos and colleagues [10]. Quantitative analysed showed approximately 25-30% co-localisation of APP with the TGN marker GCC88 following AP4μ depletion compared with <10% co-localisation in control cell (Fig. 6C). The increased level of APP localisation in the TGN in AP4μ depletion cells is similar to Arl5b depleted cells (Fig. 4D), suggesting that both Arl5b and AP4 may be involved in regulating APP transport from the TGN.

Analysis of intracellular distribution of APP in Arl5b depleted cell populations by flow cytometry

Analysis of APP intracellular distribution by microscopy is limited to a small number of cells, therefore to further verify the change in APP distribution throughout the cell population, we used a method we have recently developed to determine the intracellular location of fluorescent molecules based on the measurement of the pulse-width of a fluorescent signal by flow cytometry [34]. Pulse-width (PulSA) analysis is a multi-dimensional analysis of protein location at high speed and throughput [34,35]. Using HeLa cells stably expressing APP_{695wt}, we analysed a population of 10,000 cells depleted either of Arl5b or AP4. There was a clear difference in the pulse-width distribution of the APP after Arl5b or AP4μ depletion compared with control conditions (Fig. 7A, B). In cells depleted of either Arl5b or AP4μ, the pulse width histogram of APP showed a leftward shift compared with control cells (Fig. 7A, B) indicating a narrower width of the fluorescent signal, consistent with the localisation of a significant proportion of APP in a juxtanuclear Golgi region of the cell as compared to a broader, more disperse distribution in endosomes in the control cells. Furthermore, the median pulse width of APP in cells depleted of either Arl5b or AP4μ shifted towards the narrower pulse width of the Golgi marker, GRASP65. The pulse-width of the Golgi marker, GRASP65, was very similar between the control and Arl5b or AP4μ depleted cell population (Fig. 7C, D), indicating that the differences in pulse-width of APP was due to differences in the intracellular distribution of APP between the cell populations.

AP4 interacts with Arl5b

As the depletion of Arl5b had a similar effect as AP4 depletion on APP post-Golgi trafficking, we investigated whether Arl5b was required for the recruitment of AP4 to TGN membranes. If this was the case, then Arl5b and AP4 may interact and co-precipitate. To examine this possibility, we used HeLa cells stably expressing constitutive active Arl5b(Q70L)-GFP. Arl5b(Q70L) was used to ensure Arl5b is localized to membranes and interacts with its effectors. HeLa cells expressing Arl5b(Q70L)-GFP were lysed and Arl5b-GFP was immunoprecipitated using monoclonal antibodies to the GFP tag. Immunoprecipitated complexes were then analysed by immunoblotting for the AP4μ subunit. This analysis showed that Arl5b-GFP co-immunoprecipitated AP4μ as well as another subunit in the AP4 protein complex, AP4ε (Fig. 8A). In contrast, neither Arf1 nor AP1γ, a subunit of the AP1 adaptor protein complex localised to the TGN, were immunoprecipitated with Arl5b-GFP (Fig. 8A). In addition, the AP4μ subunit was not detected in a GFP immunoprecipitate of cell lysates from cells transfected with the GFP vector alone, confirming the specificity of the pull down (Fig. 8A). Taken together, these results suggest that Arl5b interacts specifically with AP4.

Arl5b recruits AP4 to membranes

We next examined whether Arl5b and AP4 were co-localized *in vivo*. As the antibodies to AP4μ do not detect endogenous AP4μ by immunofluorescence, we analysed the location of AP4ε. Dual localisation of Arl5b-GFP and AP4ε showed considerable overlap by confocal microscopy (Fig. 8B). As expected Arl5b also showed considerable overlap with the TGN marker GCC88, indicating that Arl5b and AP4 co-localised within the same domains of the TGN. To examine if Arl5b was required to recruit AP4 to the TGN membranes, we analysed the distribution of AP4ε following depletion of Arl5b. Silencing of Arl5b resulted in a considerable reduction of AP4ε fluorescence in the Golgi region, whereas AP4ε remained located at the Golgi after Arf1 depletion (Fig. 8B), or double knock down of Arf1 and Arf4 (data not shown). Quantitative analysis of the fluorescent intensity revealed a >50% reduction of AP4ε in the Golgi region in Arl5b siRNA treated cells (Fig. 8D) compared with cells treated with either control siRNA or Arf1 siRNA. Expression of the siRNA resistant Arl5b-GFP mutant in Arl5b siRNA treated HeLa cells rescued the recruitment of AP4ε at the Golgi region (Fig. 8C), confirming that the reduction of Golgi localised AP4 was due specifically to the depletion of Arl5b.

To further investigate if Arl5b or AP4μ depletion resulted in the dissociation of the whole AP4 complex from the TGN, we assessed the distribution of AP4 in the entire cell population using flow cytometry. As the antibodies to AP4μ do not detect endogenous AP4μ by immunofluorescence, we analysed the pulse width of AP4ε by PulSA to determine the distribution of AP4. It is likely that the depletion of the AP4μ subunit in the adaptor protein complex perturbs the assembly of the complex and thus result in dissociation of the whole AP4 complex from TGN membranes into the cytosol. PulSA analysis showed a rightward shift in the pulse width of AP4ε in HeLa cells depleted of Arl5b or AP4μ compared with control cells (Fig. 9A). This increase in the pulse width is indicative of a wider fluorescent signal width by AP4ε (Fig. 9B) suggesting that depletion of either Arl5b or AP4μ resulted in the dissociation of the AP4 complex from the TGN and AP4ε adopting a more dispersed distribution. We also analysed the pulse width of $AP1^3$ under the same conditions. PulSA did not show any changes to the $AP1^3$ pulse width in either Arl5b or AP4μ depleted cells (Fig. 9C, D) indicating that Arl5b or AP4μ depletion did not result in AP1 dissociation from the TGN in the cell population and the impact of the loss of Arl5b was specific for AP4. The pulse width of GRASP65, a marker of the Golgi did not change under conditions where Arl5b or AP4 were depleted (Fig. 9E, F) indicating that Arl5b siRNA and AP4 siRNA treatment of cells did not alter the distribution of other Golgi-localized proteins or the morphology of the Golgi which could have affected the pulse width. Collectively these results clearly show that Arl5b is required for the efficient localisation of AP4 to the Golgi.

Impact of Aβ production by Arl5b and AP4 knockdown

To assess whether Arl5b and AP4 depletion alters Aβ production, conditioned media was collected from HeLa cells stably expressing APP_{695wt}. Secreted APP processing

products produced from APP cleavage by endogenous BACE1 were analysed for the presence of Aβ using a sandwich ELISA specific for $A\beta_{40}$. The levels of Aβ for each sample were normalized against total cell protein levels. There was an approximately 2.9 and 3.2 fold increase in Aβ production in Arl5b and AP4μ depleted conditions respectively as compared to control siRNA conditions (Fig. 10A). A similar fold increase in Aβ production was also observed when AP4ε was knocked down (not shown). The level of sAPP±, a product from the non-amyloidogenic processing of APP, was very similar in all siRNA treated cells indicating that the efficiency of non-amyloidogenic processing of APP was not affected by Arl5b or AP4μ depletion (Fig. 10B, C). Given that intact APP accumulated in the TGN, this finding indicates that the non-amyloidogenic processing of APP can probably occur in multiple locations including the TGN as previously suggested [2].

A² production is a measurement of cleavage by both BACE1 and γ-secretase. To directly assess the cleavage of APP by BACE1 we performed the experiment in the presence and absence of the γ-secretase inhibitor, DAPT, and assessed the levels of β-CTF/C99, the product of APP-BACE1 cleavage. For this experiment we silenced AP4ε and immunoblotting showed a reduction in protein levels by approximately 90% (Fig. 10D). In the absence of DAPT, β-CTF/C99 was not detected in control siRNA treated cells and only at very low levels in Arl5b siRNA or AP4ε siRNA treated cells. However, in the presence of DAPT the levels of intracellular β-CTF/C99 were increased (Fig 10D) and there was a 3-fold increase in the level of β-CTF/C99 in Arl5b siRNA or AP4ε siRNA treated cells compared with control siRNA treated cells (Fig. 10D, E). The increase in the level of the β-CTF/C99 product demonstrates enhanced intracellular cleavage of APP by BACE1 following depletion of the TGN localised components Arl5b and AP4.

Taken together, these results demonstrate that both Arl5b and AP4 are important in the regulation of APP trafficking from the TGN and are required to regulate Aβ production. In addition, these results further supports that the Golgi is a compartment where APP can be processed and result in Aβ production.

Discussion

The intracellular itinerary of APP is important in the regulation of its proteolytic processing by BACE1 and γ-secretase. The initial cleavage of APP by BACE1 is the rate limiting step in the generation of Aβ and a target for therapeutic intervention. Several AD susceptibility genes are associated with the regulation of membrane trafficking [36-42] and there is emerging evidence in experimental animal models that defective membrane trafficking contributes to AD [43-45]. In particular, dysfunctional endosomal trafficking of APP and BACE1 has attracted considerable attention over the past few years as an underlying defect associated with enhanced Aβ generation. However, in addition to Aβ generation in the endo/lysosomal system there have been numerous studies to indicate that A² can also generated in the secretory pathway [8-12,29]. The TGN is a slightly acidic compartment that provides favourable conditions for cleavage of APP by BACE1. Given the co-transport of newly synthesised APP and BACE1 along the secretory pathway it is important to understand the machinery for post-Golgi export and the transport route of APP from the Golgi to the endosomes.

Here we have examined the post-Golgi transport of APP and have shown that (1) APP traffics from the TGN directly to the early endosomes. Notably, very few if any cargo have been identified to take this route as the classical pathway for newly synthesised cargo to reach the early endosomes is via the PM; (2) the small G protein, Arl5b and adaptor protein complex, AP4, both localised to the TGN [32,46,47] are essential for Golgi export of APP; (3) Arl5b is required for the recruitment of AP4 to TGN membranes; (4) depletion of either Arl5b or AP4 by RNAi results in an accumulation of APP in the Golgi and increased Aβ production, hence the residency time of APP in the TGN influences its processing; and (5) accumulation of APP in the TGN resulted in an increase in secreted Aβ, indicating that Aβ produced in the Golgi is readily secreted from the cell. Overall our findings show that the efficiency of post-Golgi trafficking of newly synthesised APP is an important factor in regulating its processing by secretases.

In contrast to a number of other studies analysing APP trafficking which have used transient overexpression of APP, here we generated and employed a stable cell line expressing APP at only modest levels to minimize the consequence of saturation of the trafficking machinery at the Golgi and post-Golgi compartments. The anterograde transport of APP was tracked in the stably expressing APP_{695wt} HeLa cells following treatment with CHX to inhibit protein synthesis. Our previous study demonstrated that APP or a chimeric CD8/APP molecule containing the cytoplasmic tail of APP had a relatively short half-life and was trafficked to the lysosome for degradation [29]. A four hour treatment with CHX treatment was sufficient to allow turnover of the existing pool of APP, and after washing cells free of CHX, we then tracked the post-Golgi transport of newly synthesised APP. The wave of newly synthesised APP localized predominantly to the Golgi complex one hour after protein synthesis resumed, and the localization of this wave subsequently shifted to the early endosomes. The movement of APP from the TGN to the early endosomes and not the late endosomes, or the recycling endosomes, supports the conclusion of a direct transport of APP from the TGN to the early endosomes. At a later time point the wave of APP was also detected in Rab7+ late endosome compartment. The addition of Pitstop 2 to inhibit AP2/clathrin mediated endocytosis did not increase the level of APP at the PM, indicating that the pool of APP in the late endosomes is derived from transport of APP directly from the early endosomes. APP did not traffic through the recycling endosomes demonstrating that newly synthesised APP is excluded from the pathway that transports cargo to the PM via

the recycling endosomes. Two hours following CHX removal the distribution of APP in the Golgi/early endosomes/late endosomes was very similar to the steady state distribution of APP in the stable HeLa cell line (Fig. 1C), implying that the transport route of this wave of newly synthesised APP recapitulated the normal trafficking route for this cargo.

Of note is that very little APP was detected at the cell surface either under steady state conditions or by tracking the newly synthesised APP, a finding consistent with reports in the literature [48]. Our finding that the major pathway of APP transport from the Golgi is to the early endosomes and then to the late endosomes, and not to the cell surface, highlights the importance of post-Golgi export of APP in the delivery to the endo/lysosomal system. Hence, endocytosis of APP from the PM to the early endosomes is probably a minor pathway for the delivery of APP to the endosomal system.

AP4 has previously been shown to interact with the YKFFE sorting motif on APP via the μ subunit [10] and to regulate the post-Golgi trafficking of APP from the TGN to the endosomes [10]. However, this earlier study did not identify whether the compartment was an early, late or recycling endosome and did not determine whether the transport was direct or indirect to the endosomal compartment. Here we have confirmed the importance of AP4 using a APP_{695wt} expressing HeLa cell line and showed that APP is transported directly from the TGN to the early endosomes. Although Arf1 has previously been reported to interact with AP4 in yeast-2-hybrid studies [26], it was unknown whether Arf1 could interact and recruit AP4 in mammalian cells. We were unable to detect any change in the distribution of APP following Arf1 depletion or Arf1+ Arf4 depletion *in vivo*. We interpret these findings that AP4 recruitment to the Golgi does not require Arf1 and this raised the possibility of another small G protein responsible for recruiting AP4 to the TGN membranes.

In a previous study, Arl5b was shown to localise to the TGN and the silencing of Arl5b slows down trafficking of cargos from endosomes to the TGN [32]. Based on these observations we had proposed that Arl5b may mediate the transport of machinery from the TGN to the endosomes which would account for the reduced efficiency of retrograde transport from endosomes to the TGN [32]. Here we have shown that Arl5b is required for Golgi export of APP. Arl5b depletion, like AP4μ depletion, resulted in a similar shift in APP distribution and an increase in APP located at the TGN. This conclusion was based on both quantitative analysis of optical images as well as the use of a flow cytometry to analyse the pulse width of the fluorescent signal in the entire cell population. The increase of the non-cleavable CD8/APP in the TGN following Arl5b depletion confirms that the transport block in the absence of Arl5b is dependent on the cytoplasmic tail of APP. Arl5b is essential for the recruitment of AP4 to TGN membranes. By microscopy and PulSA flow cytometric analysis we showed that Arl5b depletion resulted in the dissociation of AP4 from the TGN membranes. In addition, Arl5b or AP4 depletion did not affect the localization of AP1, another adaptor protein complex localized to the TGN. Caster and Kahn [49] reported that short term brefeldin A treatment did not influence AP4 staining patterns, which is consistent with the behaviour of Arl5b and not Arf1, as Arl5b dissociates from the Golgi slowly after brefeldin A treatment compared with Arf1 (Houghton and Gleeson, unpublished data). We also showed that two different subunits of AP4 were co-immunoprecipitate with Arl5b-GFP demonstrating an interaction between Arl5b and the AP4 protein complex. The absence of Arf1 or AP1 in the Arl5b-GFP pulldown further supports that the interaction of Arl5b with AP4 is specific. However, whether the interaction is direct or indirect remains to be shown.

In contrast to APP, Arl5b depletion did not affect the distribution of BACE1 indicating that the machinery and transport pathways that regulate APP and BACE1 export from the TGN differ, as outlined in the proposed model in Fig. 11. Sorting of BACE1 and APP into distinct pathways would provide a mechanism for segregation of these two membrane proteins at the TGN and thereby reducing the extent of BACE1 mediated processing of APP.

Our study indicates that AP4-mediated Golgi export represents a major pathway for delivery of APP cargo to the endosomal system. Upon depletion of either Arl5b or AP4μ it was noted there was residual APP in punctate endosomal structures. This could be due to incomplete depletion of machinery component or a consequence of TGN export mediated by an AP4-independent pathway. One possibility is the involvement of Mint adaptors [49] which are localized to multiple locations such as the TGN, ER or plasma membrane [27]. In particular, Mint3 has been shown to bind to the GYENPTY motif in cyotoplasmic tail of APP and Mint3 is recruited to the Golgi following transient expression of APP in HeLa cells [49]. These authors reported a rapid Golgi export of APP in transiently transfected cells to the $LAMP1^+$ endosomes, a finding that is difficult to reconcile with the location of the major fraction of APP to early endosomes under steady state conditions. A major difference in the previous study by Caster and Kahn [49] is the use of a transient transfection system in their study which is likely to result a higher level of APP expression and, given that AP4 levels are low in HeLa cells, the Arl5b/AP4 sorting system may be readily saturated upon high expression of APP. Our findings show that, at a modest level of expression, APP is transported to the early endosomes in an AP4-dependent pathway, and given the report by Caster and Kahn [49] we suggest that at higher levels of expression excess APP may be transported directly to late endosomes/lysosomes via the Mint3 dependent pathway.

The current data also lends further support for a contribution of the secretory pathway in the generation of Aβ. There was enhanced processing of APP in AP4 and Arl5b depleted cells as revealed by a 2.9 and 3.2-fold increase in A^2 secretion, respectively, compared with control siRNA treated cells. Moreover, there was a 3-fold increase in the level of β-CTF/C99 in either AP4 or Arl5b depleted cells in the presence of the γ-secretase inhibitor, confirming an increased BACE1-mediated cleavage of APP when APP export is blocked from

the TGN. This result strongly implies that BACE1 can cleave APP in the TGN compartment and is consistent with our earlier report where APP cleavage was enhanced in cells expressing a BACE1 chimera which recycled via the TGN rather than recycling endosomes [29] and also findings from other groups [10,11]. In addition, the observation that only low levels of β-CTF/C99 were detected in AP4-depleted cells in the absence of the γ-secretase inhibitor indicates that processing of β-CTF/C99 by γ-secretase is efficient in Arl5b and AP4 depleted cells, and that cleavage by γ-secretase is also likely to occur in the TGN. Aβ peptide generated in the TGN could then be secreted from the cell by a variety of anterograde transport pathways to the PM. Overall our findings demonstrate that a block in the trafficking machinery that regulates APP exit from the TGN results in a build up of APP in the TGN which in turn may then result in a loss of partitioning between APP and newly synthesised BACE1 arriving at the TGN, which would account for an increased proteolytic processing of APP.

In conclusion, the results presented here have identified that Arl5b interacts and recruits AP4 to the TGN and regulates APP anterograde transport from the TGN to the early endosomes. To the authors knowledge this is the first example of the AP4 adaptor involved in cargo transport specifically to the early endosomes. Excessive build up of APP in the TGN results in APP processing and secretion of Aβ, highlighting the potential importance of the acidic TGN compartment as a site for Aβ production. On the other hand, export of BACE1 from the TGN is independent of the Arl5b/AP4 sorting machinery indicating that APP and BACE1 are segregated into distinct post-Golgi transport pathways (Fig. 11). Hence AP4 and Arl5b are likely to play a role in mediating the segregation of APP from BACE1 in the secretory pathway, a process that could partition the enzyme and substrate into two membrane domains to minimize the level of A² generated in the TGN. These findings highlight the complexity of APP transport pathways and the need to consider multiple intracellular sites for APP processing.

Materials and Methods

Plasmids, antibodies

pIRESpuro-APP_{695wt} was a gift from Prof. Andrew F. Hill, La Trobe University, Victoria, Australia [50]. pCI-Neo-CD8-APP_{695wt} has been described previously [29]. Rabbit polyclonal antibodies to GCC88 have been described [51,52]. Mouse monoclonal antibodies to AP4ε-subunit (Clone 32) and AP1 γ-adaptin (Clone 88) were purchased from Transduction laboratories (BD Biosciences, North Ryde, NSW, Australia). Mouse monoclonal antibodies to CD8 (Clone RPA-T8) was from eBioscience (San Diego, CA, USA). Rabbit polyclonal antibodies to Arf1 (ARFS-3F1), AP4 μ–subunit (ab96306) and GRASP 65 (ab30315) were obtained from Abcam (Cambridge, UK). Rabbit polyclonal antibodies to EEA1 (#2411), Rab11 (#5589) and Rab7 (#9367) were from cell signalling technology (Danvers, MA, USA). Rabbit polyclonal to ²-secretase (BACE1) (Clone EE17) was obtained from Sigma Aldrich (Castle Hill, NSW, Australia). Rabbit antibodies to Arf4 were from ProteinTech (Cat no#11673-1-AP) (Rosemont, IL, USA). Mouse antibodies to ±-tubulin (Clone 236-10501), golgin97 (A-21270), rabbit polyclonal antibodies to GFP (A6455) and mouse monoclonal to amyloid precursor protein (APP) (Clone NAB228) were from Life Technologies (Grand Island, NY, USA). Mouse monoclonal antibodies to Aβ4-10 (Clone WO_2) were from Merck Millipore (Australia). Rabbit antibodies to the C-terminal 20 amino acids of APP were purchased from Merck Millipore/Calbiochem (Catalogue #171610).

Secondary antibodies used for immunofluorescence were goat anti-rabbit IgG-Alexa Fluor 568 nm, goat anti-rabbit IgG-Alexa Fluor 488 nm, goat anti-mouse IgG-Alexa Fluor 568 nm and goat anti-mouse IgG-Alexa Fluor 488 nm, and purchased from Life Technologies (Grand Island, NY, USA). Horse-radish peroxidase (HRP)-conjugated sheep anti-rabbit Ig and anti-mouse Ig were purchased from DAKO Corporation (Carpinteria, CA, USA).

Cell culture and transient transfections

HeLa cells were maintained as a semi-confluent monolayer in Dulbecco's Modified Eagle's media (DMEM) supplemented with 10% (v/v) fetal calf serum (FCS), 2 mM glutamine and 100 units/μL penicillin and 0.1% streptomycin (C-DMEM). For transient transfections, HeLa cells were seeded as monolayers in 12-well plates with coverslips. Cells were transfected with plasmid DNA (0.3-1.0 μg/well) using FuGene 6 (Promega, USA) according to manufacturer's protocol. Transfected cells were cultured for 24-72 h.

For some experiments, cells were incubated with 30 μM Pitstop 2 (Abcam, Cambridge, UK) or 250 nM N-[N-(3,5 diflourophenacetyl-L-alanyl)]-S-phenylglycine t-butyl ester (DAPT) (Sigma-Aldrich).

Generation of stable cell line

A HeLa cell line stably expressing APP_{695wt} was generated by transfecting wild-type HeLa cells with the pIRESpuro-APP_{695wt} construct using FuGene 6 (Roche, USA). Stably expressing cells were selected in C-DMEM (Life Technologies, USA) with 1 μg/mL puromycin (Invitrogen, USA). Monoclonal cell lines were obtained using limit dilution and resultant cell populations screened by immunofluorescence and immunoblotting. The stable cell line was maintained in C-DMEM with 500 ng/mL puromycin.

RNA interference

For short interfering RNA (siRNA) transfections, cell monolayers were transfected with siRNA (0.08 μM/well) using Dharmafect 1 (Thermo-Fisher, USA) according to the manufacturer's protocol. Transfected cells were incubated for 72 h at 37 °C, 10 % CO_2. Arl5b-1 and Arl5b-2 specific siRNA duplexes were described by Houghton *et al* [32]. AP4μ-1 siRNA has been described by Janvier *et al* [53] and AP4μ-2 siRNA was

as follows: CGCAAUGUGGCUCUGGUAU. AP4ε-1 and AP4ε-2 siRNAs (Sigma-Proligo database) were CUUGAUGAAUCCUUACGAA and GGCAUAUGAAGAUGAUUAU. Arf1-1 siRNA has been described [54] and Arf1-2 siRNA was GCCUGAUCUUCGUGGUGGA (Sigma-Proligo database). Arf4 siRNAs (Sigma-Proligo database) were CAGAAUACCCAGGGUCUUA and GAUGUUGGUGGUCAAGAUA. All duplex siRNAs were synthesised by Sigma-Proligo (Australia).

Quantitative Real Time Polymerase Chain Reaction (q-RT-PCR)

Total RNA was isolated with the Qiagen RNeasy mini kit (Qiagen, Doncaster, Vic, Australia) from ~2 × 10^5 cells cultured in 6 well plates that were either untreated, or transfected with control siRNA or AP4μ-1 or AP4μ-2 siRNA for 72 h. RNA preparations were treated with Turbo DNase. Total RNA (2 μg) was converted to cDNA using a SuperScript® III First-Strand Synthesis kit (Life-Technologies). cDNA (1/10 dilution) was used with Taqman Fast Advanced Master mix and human specific Taqman Gene Expression Assays (Applied Biosystems) to setup 20 μl singleplex reactions in quadruplicate for AP4μ (Hs00428095_m1), with internal endogenous reference genes for human GAPDH (Hs02758991_g1). qPCR reactions were then run on a StepOnePlus qPCR machine (Applied Biosystems) and analysed using the comparative DeltaDelta CT method. Relative quantification of mRNA levels used control siRNA cells as the normaliser and *GAPDH* as the internal reference genes. Analyses were performed in quadruplicate for each gene. Data is represented as the mean± SEM of three experiments.

Indirect immunofluorescence

Monolayers on coverslips were fixed in 4% paraformaldehyde (PFA) for 15 min at room temperature, followed by quenching in 50 mM NH_4Cl/PBS for 10 min at RT. Cells were permeablized with 0.1% Triton X-100/PBS for 4 min and blocked in Blocking Solution (5% FCS, 0.02% Sodium Azide in PBS) for 30 min to reduce non specific binding. The above was used for all staining except for AP4ε staining, where cells were fixed and permeabilized using 100% methanol at -20 ˚C for 5 min, then blocked in Blocking Solution for 30 min and for AP-1γ staining, where cells were fixed in 4% PFA for 15 min and permeabilized in 0.1% Triton X-100/PBS for 15 min, then blocked in 1% BSA/0.3% Triton X-100/PBS. Cells were incubated with primary antibodies diluted in blocking solution for 1 h at room temperature and washed 6 times in PBS. Diluted fluorochrome-conjugated secondary antibodies were added to monolayers and incubated for 30 min at RT before washed 6 times in PBS. Coverslips were washed in milli-Q water before mounting in Mowiol. Confocal microscopy was performed using a Leica TCS SP2 or SP8 system. Images were collected sequentially for multi-colour imaging.

Analysis of AP4ε fluorescence in Golgi versus Cytoplasm

FIJI (ImageJ) was used for image analysis. To calculate the fluorescence signal of AP4ε at the TGN compared with the cytoplasm in stained HeLa cells, a TGN mask and nuclear mask were generated using GCC88 and DAPI specific fluorescence signals, respectively, using FIJI (ImageJ). The AP4μ fluorescence intensity in the TGN and nuclear mask was then subtracted from the total fluorescence intensity of AP4μ in the cell to obtain the AP4μ fluorescence signal in the cytoplasm. The fluorescence signal of AP4μ at the TGN is expressed as a ratio of the fluorescence signal of AP4μ in the cytoplasm. All fluorescence images were collected with the Leica SP8 microscope using identical settings.

Immunoblotting

Samples with equal cell number were lysed in 4x reducing sample buffer and boiled for 5 min at 100 °C. Protein concentration was determined using the Bradford assay. Proteins were resolved on a SDS-PAGE polyacrylamide gel (Life Technologies, USA) and transferred onto Immobilon-P polyvinylidene fluroride (PVDF) membrane (Millipore, NSW, Australia) at 30 V overnight at 4 °C. The membrane was blocked by drying at 37 °C. The membrane was incubated with primary antibodies diluted in 5 % skim milk/PBS for 1 h and then washed three times for 10 min each in 0.1% (v/v) PBS-Tween 20. Horse radish peroxidase (HRP)-conjugated secondary antibodies were then added to the membrane for 1h and washed as above. Bound antibodies were detected using chemiluminescence and captured using the Gel-Pro™ Analyser version 4.5 software (MediaCybernetics, Berthesda, MD, USA). Densitometry of the protein bands were measured using the Gel-Pro™ Analyser program.

To detect ²-CTF/C99 fragment levels, cell lysates from HeLa cells stably expressing APP_{695wt} were mixed with 4x buffer containing 20% ²-mercaptoethanol and boiled for 10 min at 100 °C. Samples were resolved on a 12% Bis-Tris SDS-PAGE polyacrylamide gel (Life Technologies, USA) and transferred onto 0.2 μm nitrocellulose membrane (Bio-Rad, Australia) at 400 mA for 1 h on ice. The membrane was then blocked with 10% milk/ PBS-Tween 20 for 1h, room temperature to reduce unspecific binding before incubated overnight at 4 °C in affinity purified WO-2 antibodies diluted in PBS-Tween 20 (1/6000). The membrane was washed three times for 10 min each in PBS-Tween 20. HRP-conjugated secondary antibodies were then added to the membrane for 1 h and washed as above. Bound antibodies were detected using chemiluminescence and captured using the Gel-Pro™ Analyser version 4.5 software (MediaCybernetics, Berthesda, MD, USA). Densitometry of the protein bands were measured using the Gel-Pro™ Analyser program.

Anterograde transport assay of APP

HeLa cells stably expressing APP_{695wt} were treated with 50 μg/mL cycloheximide (CHX) for 4 h, washed twice with PBS and incubated in C-DMEM at 37 °C for the

indicated time points up to 2 h. Cells harvested at each time point were fixed with 4% PFA and stained.

Pulse Width Analysis (PulSA) and flow cytometry

Monolayers of HeLa cells stably expressing APP_{695wt} were lifted by incubation with 5 mM EDTA/PBS for 15 min, at RT. For pulse width analysis (PulSA), cells were fixed with 4% PFA, quenched with 50 mM NH_4Cl, permeablized with 0.1% Triton X-100 for 4 min in suspension and blocked in Blocking Solution (5% FCS, 0.02% Sodium Azide in PBS). Cells were incubated with primary antibodies followed by addition of fluorophore-conjugated secondary antibodies. For detection of cell surface membrane proteins, live cells were stained in suspension with antibodies for 30 min on ice before being fixed with 4% PFA, quenched with 50 mM NH_4Cl and blocked in Blocking Solution (5% FCS, 0.02% sodium azide in PBS) for 30 min. Antibody-bound complexes were detected by addition of fluorophore-conjugated secondary antibodies.

Cells were analysed at a medium flow rate in an LSRFortessa flow cytometer, equipped with 405 nm, 488 nm, 561nm and 640nm lasers (BD Biosciences). Approximately 10, 000 events were collected, using a forward scatter threshold of 5000. For PulSA analysis, data were collected for pulse height, area and width parameters for each channel as previously described [34,35].

Immunoprecipitation

Untransfected HeLa cells and HeLa cells stably expressing Arl5b (Q70L)-GFP were grown as monolayers in 10 cm tissue culture dishes. Cells (10^7) were harvested by trypsinization and washed twice in cold PBS. Immunoprecipitation was carried using a GFP-Trap® kit (Chromatek, Germany) according to manufacturer's protocol. Briefly, cells were lysed for 30 min on ice with RIPA buffer (1 mM Tris/Cl pH 7.5; 15 mM NaCl; 0.5 mM EDTA; 0.01% SDS; 0.1% Triton X-100; 0.1% Deoxycholate) provided by the kit. Cell lysates were incubated with the magnetic beads for 2 h at 4 °C. Bound antibody complexes were eluted from the beads by boiling in 4x sample reducing buffer for 5 min at 100 °C and analysed by SDS-PAGE followed by immunoblotting with appropriate antibodies.

A² ELISAs

Secreted $A²_{40}$ levels from overnight conditioned media were measured using an $A²_{40}$ specific A² ELISA kit (Life Technologies, USA) as per manufacturer's protocol. Secreted A² levels were normalized against total protein concentrations of cell lysates as measured using a Bradford assay.

Quantitation of co-localisation and statistical analysis

Quantitation of the co-localization between internalized cargo and fluorescent organelle markers was performed using the plugin organelle-based co-localization (OBCOL) [55] on the Image J program (NIH public domain software). Quantitation was carried out for the indicated number of cells at each time point. The percentage of cargo stained with various organelle-specific antibodies was calculated by taking the sum of overlapping pixels between the cargo and the different markers, divided by the total number of cargo pixels within each cell. All analyses included samples from two or more independent experiments. Data was expressed as the mean, ± SEM and analysed by either an unpaired, two-tailed, student *t*-test or in the case of the qPCR data analysed by a paired, two-tailed student *t*-test. A $p < 0.05$(*) was considered significant, $p < 0.01$ (**) was highly significant and $p < 0.001$ (***) was very highly significant. An absence of a *p* value indicates that the differences were not significant.

Acknowledgements

This work was supported by funding from the National Health and Medical Research Council of Australia. WHT, JZAT and KLZ are supported by University of Melbourne International Graduate Scholarships. The authors acknowledge the facilities and technical assistance of The Biological Optical Microscopy Platform (BOMP) at the University of Melbourne.

The authors declare no conflict of interest.

References

1. Sisodia SS. Beta-amyloid precursor protein cleavage by a membrane-bound protease. *Proc Natl Acad Sci U S A.* 1992;89(13):6075-6079.
2. Skovronsky DM, Moore DB, Milla ME, Doms RW, Lee VMY. Protein kinase C-dependent alpha-secretase competes with beta-secretase for cleavage of amyloid-beta precursor protein in the trans-Golgi network. *Journal of Biological Chemistry.* 2000;275(4):2568-2575.
3. Thinakaran G, Koo EH. Amyloid precursor protein trafficking, processing, and function. *J Biol Chem.* 2008;283(44):29615-29619.
4. Kinoshita A, Fukumoto H, Shah T, Whelan CM, Irizarry MC, Hyman BT. Demonstration by FRET of BACE interaction with the amyloid precursor protein at the cell surface and in early endosomes. *J Cell Sci.* 2003;116(Pt 16):3339-3346.
5. Koo EH, Squazzo SL, Selkoe DJ, Koo CH. Trafficking of cell-surface amyloid beta-protein precursor. I. Secretion, endocytosis and recycling as detected by labeled monoclonal antibody. *J Cell Sci.* 1996;109 (Pt 5):991-998.
6. Rajendran L, Honsho M, Zahn TR, et al. Alzheimer's disease beta-amyloid peptides are released in association

with exosomes. *Proc Natl Acad Sci U S A.* 2006;103(30):11172-11177.
7. Small SA, Gandy S. Sorting through the cell biology of Alzheimer's disease: intracellular pathways to pathogenesis. *Neuron.* 2006;52(1):15-31.
8. Xu H, Sweeney D, Wang R, et al. Generation of Alzheimer beta-amyloid protein in the *trans*-Golgi network in the apparent absence of vesicle formation. *Proc Natl Acad Sci U S A.* 1997;94(8):3748-3752.
9. Siman R, Velji J. Localization of presenilin-nicastrin complexes and gamma-secretase activity to the trans-Golgi network. *J Neurochem.* 2003;84(5):1143-1153.
10. Burgos PV, Mardones GA, Rojas AL, et al. Sorting of the Alzheimer's disease amyloid precursor protein mediated by the AP-4 complex. *Dev Cell.* 2010;18(3):425-436.
11. Choy RW, Cheng Z, Schekman R. Amyloid precursor protein (APP) traffics from the cell surface via endosomes for amyloid beta (Abeta) production in the trans-Golgi network. *Proc Natl Acad Sci U S A.* 2012;109(30):E2077-E2082.
12. Huse JT, Doms RW. Neurotoxic traffic: uncovering the mechanics of amyloid production in Alzheimer's disease. *Traffic.* 2001;2(2):75-81.
13. Toh WH, Gleeson PA. Dysregulation of intracellular trafficking and endosomal sorting in Alzheimer's disease: controversies and unanswered questions. *Biochem J.* 2016;473(14):1977-1993.
14. Walter J, Haass C. Posttranslational modifications of amyloid precursor protein : ectodomain phosphorylation and sulfation. *Methods Mol Med.* 2000;32:149-168.
15. De Matteis MA, Luini A. Exiting the Golgi complex. *Nat Rev Mol Cell Biol.* 2008;9(4):273-284.
16. Goud B, Gleeson PA. TGN golgins, Rabs and cytoskeleton: regulating the Golgi trafficking highways. *Trends Cell Biol.* 2010;20(6):329-336.
17. Robinson MS. Adaptable adaptors for coated vesicles. *Trends in Cell Biology.* 2004;14(4):167-174.
18. Lock JG, Hammond LA, Houghton F, Gleeson PA, Stow JL. E-cadherin transport from the trans-Golgi network in tubulovesicular carriers is selectively regulated by golgin-97. *Traffic.* 2005;6(12):1142-1156.
19. Lieu ZZ, Lock JG, Hammond LA, La Gruta NL, Stow JL, Gleeson PA. A trans-Golgi network golgin is required for the regulated secretion of TNF in activated macrophages in vivo. *Proc Natl Acad Sci U S A.* 2008;105(9):3351-3356.
20. Kametaka S, Waguri S. Visualization of TGN-endosome trafficking in mammalian and Drosophila cells. *Methods Enzymol.* 2012;504:255-271.
21. Schmid SL. Clathrin-coated vesicle formation and protein sorting: an integrated process. *Annu Rev Biochem.* 1997;66:511-548.
22. Marks MS, Woodruff L, Ohno H, Bonifacino JS. Protein targeting by tyrosine- and di-leucine-based signals: evidence for distinct saturable components. *J Cell Biol.* 1996;135(2):341-354.
23. Borg JP, Ooi J, Levy E, Margolis B. The phosphotyrosine interaction domains of X11 and FE65 bind to distinct sites on the YENPTY motif of amyloid precursor protein. *Mol Cell Biol.* 1996;16(11):6229-6241.
24. Nordeng TW, Bakke O. Overexpression of proteins containing tyrosine- or leucine-based sorting signals affects transferrin receptor trafficking. *J Biol Chem.* 1999;274(30):21139-21148.
25. Lee MS, Kao SC, Lemere CA, et al. APP processing is regulated by cytoplasmic phosphorylation. *J Cell Biol.* 2003;163(1):83-95.
26. Boehm M, Aguilar RC, Bonifacino JS. Functional and physical interactions of the adaptor protein complex AP-4 with ADP-ribosylation factors (ARFs). *EMBO J.* 2001;20(22):6265-6276.
27. Rogelj B, Mitchell JC, Miller CC, McLoughlin DM. The X11/Mint family of adaptor proteins. *Brain research reviews.* 2006;52(2):305-315.
28. Miller CC, McLoughlin DM, Lau KF, Tennant ME, Rogelj B. The X11 proteins, Abeta production and Alzheimer's disease. *Trends Neurosci.* 2006;29(5):280-285.
29. Chia PZ, Toh WH, Sharples R, Gasnereau I, Hill AF, Gleeson PA. Intracellular Itinerary of Internalised beta-Secretase, BACE1, and Its Potential Impact on beta-Amyloid Peptide Biogenesis. *Traffic.* 2013;14(9):997-1013.
30. von Kleist L, Stahlschmidt W, Bulut H, et al. Role of the clathrin terminal domain in regulating coated pit dynamics revealed by small molecule inhibition. *Cell.* 2011;146(3):471-484.
31. Nakai W, Kondo Y, Saitoh A, Naito T, Nakayama K, Shin HW. ARF1 and ARF4 regulate recycling endosomal morphology and retrograde transport from endosomes to the Golgi apparatus. *Molecular Biology of the Cell.* 2013;24(16):2570-2581.
32. Houghton FJ, Bellingham SA, Hill AF, et al. Arl5b is a Golgi-localised small G protein involved in the regulation of retrograde transport. *Exp Cell Res.* 2012;318(5):464-477.
33. Chia PZ, Toh WH, Sharples R, Gasnereau I, Hill AF, Gleeson PA. Intracellular Itinerary of Internalised beta-Secretase, BACE1, and Its Potential Impact on beta-Amyloid Peptide Biogenesis. *Traffic.* 2013.
34. Chia PZ, Ramdzan YM, Houghton FJ, Hatters DM, Gleeson PA. High-throughput quantitation of intracellular trafficking and organelle disruption by flow cytometry. *Traffic.* 2014;15(5):572-582.
35. Toh WH, Houghton FJ, Chia PZ, Ramdzan YM, Hatters DM, Gleeson PA. Application of flow cytometry to analyze intracellular location and trafficking of cargo in cell populations. *Methods in molecular biology.* 2015;1270:227-238.
36. Vardarajan BN, Bruesegem SY, Harbour ME, et al. Identification of Alzheimer disease-associated variants in genes that regulate retromer function. *Neurobiol Aging.* 2012;33(9):2231 e2215-2231 e2230.
37. Ginsberg SD, Mufson EJ, Alldred MJ, et al. Upregulation of select rab GTPases in cholinergic basal forebrain neurons in mild cognitive impairment and

Alzheimer's disease. *Journal of chemical neuroanatomy.* 2011;42(2):102-110.
38. Small SA, Kent K, Pierce A, et al. Model-guided microarray implicates the retromer complex in Alzheimer's disease. *Ann Neurol.* 2005;58(6):909-919.
39. Muhammad A, Flores I, Zhang H, et al. Retromer deficiency observed in Alzheimer's disease causes hippocampal dysfunction, neurodegeneration, and Abeta accumulation. *Proc Natl Acad Sci U S A.* 2008;105(20):7327-7332.
40. Rogaeva E, Meng Y, Lee JH, et al. The neuronal sortilin-related receptor SORL1 is genetically associated with Alzheimer disease. *Nat Genet.* 2007;39(2):168-177.
41. Scherzer CR, Offe K, Gearing M, et al. Loss of apolipoprotein E receptor LR11 in Alzheimer disease. *Arch Neurol.* 2004;61(8):1200-1205.
42. Andersen OM, Reiche J, Schmidt V, et al. Neuronal sorting protein-related receptor sorLA/LR11 regulates processing of the amyloid precursor protein. *Proc Natl Acad Sci U S A.* 2005;102(38):13461-13466.
43. Small SA, Petsko GA. Retromer in Alzheimer disease, Parkinson disease and other neurological disorders. *Nat Rev Neurosci.* 2015;16(3):126-132.
44. Siegenthaler BM, Rajendran L. Retromers in Alzheimer's disease. *Neuro-degenerative diseases.* 2012;10(1-4):116-121.
45. Berman DE, Ringe D, Petsko GA, Small SA. The use of pharmacological retromer chaperones in Alzheimer's disease and other endosomal-related disorders. *Neurotherapeutics : the journal of the American Society for Experimental NeuroTherapeutics.* 2015;12(1):12-18.
46. Dell'Angelica EC, Mullins C, Bonifacino JS. AP-4, a novel protein complex related to clathrin adaptors. *J Biol Chem.* 1999;274(11):7278-7285.
47. Hirst J, Bright NA, Rous B, Robinson MS. Characterization of a fourth adaptor-related protein complex. *Mol Biol Cell.* 1999;10(8):2787-2802.
48. Haass C, Kaether C, Thinakaran G, Sisodia S. Trafficking and proteolytic processing of APP. *Cold Spring Harbor perspectives in medicine.* 2012;2(5):a006270.
49. Caster AH, Kahn RA. Recruitment of the Mint3 adaptor is necessary for export of the amyloid precursor protein (APP) from the Golgi complex. *J Biol Chem.* 2013;288(40):28567-28580.
50. White AR, Du T, Laughton KM, et al. Degradation of the Alzheimer disease amyloid beta-peptide by metal-dependent up-regulation of metalloprotease activity. *J Biol Chem.* 2006;281(26):17670-17680.
51. Luke MR, Brown DL, Stow JL, Gleeson PA. Two mammalian GRIP-domain proteins, GCC88 and golgin97, exist as homo-dimers and are recruited to distinct sub-compartments of the TGN. *Mol Biol Cell.* 2003;14 supplement:106a.
52. Luke MR, Kjer-Nielsen L, Brown DL, Stow JL, Gleeson PA. GRIP domain-mediated targeting of two new coiled-coil proteins, GCC88 and GCC185, to subcompartments of the trans-Golgi network. *J Biol Chem.* 2003;278(6):4216-4226.
53. Janvier K, Bonifacino JS. Role of the endocytic machinery in the sorting of lysosome-associated membrane proteins. *Mol Biol Cell.* 2005;16(9):4231-4242.
54. Southon A, Greenough M, Hung YH, Norgate M, Burke R, Camakaris J. The ADP-ribosylation factor 1 (Arf1) is involved in regulating copper uptake. *Int J Biochem Cell Biol.* 2011;43(1):146-153.
55. Woodcroft BJ, Hammond L, Stow JL, Hamilton NA. Automated organelle-based colocalization in whole-cell imaging. *Cytometry A.* 2009;75(11):941-950.

Figure Legends

Figure 1: Post-Golgi transport of APP
(**A**) Outline of experimental plan used to track the anterograde transport of APP. (**B**) HeLa cells stably expressing APP_{695wt} untreated (no CHX) or treated with 50 µg/mL cycloheximide (CHX) for 4 h, monolayers then washed twice with PBS and protein synthesis resumed by incubating cells in C-DMEM at 37 ºC. Cells were fixed at different time points over a 2 h period following CHX washout as indicated. Monolayers were permeabilized, blocked and stained with mouse monoclonal anti-human APP antibodies (red) and rabbit polyclonal antibodies to either GCC88, EEA1 or Rab7 (green) and DAPI (blue). Inset shows magnified images. Bar represent 10 µm. (**C-D**) The percentage of APP at the TGN, early endosomes, late endosomes or recycling endosomes at each time point calculated from the percentage of total APP pixels that overlapped with GCC88, EEA1, Rab7 (C) or Rab11 (D) respectively. All calculations were performed using the OBCOL plugin on ImageJ (n=15 for each marker and time point from three independent experiments). Error bars represent SEM.

Figure 2: Newly synthesised APP is transported directly from the early endosomes to the late endosomes
(**A**) Outline of experimental plan to investigate if newly synthesised APP can be directly transported from early endosomes to the late endosomes. (**B**) HeLa cells stably expressing APP_{695wt} treated with 50 µg/mL cycloheximide (CHX) for 4 h, monolayers were then washed twice with PBS and protein synthesis was resumed by incubating cells in C-DMEM at 37 ºC. Pitstop 2 or DMSO (carrier control) was added 1 h 15 min into the recovery time and incubated for a further 45 min. Cells were fixed at the indicated time points, monolayers then permeabilized, blocked and stained with mouse monoclonal anti-human APP antibodies (red) and rabbit polyclonal antibodies to either EEA1 or Rab7 (green) and DAPI (blue). Bar represents 10 µm. (**C**) The percentage of APP at the early endosomes, or late endosomes at each time point and condition was calculated from the percentage of total APP pixels that overlapped with EEA1 or Rab7 respectively. All calculations were performed using the OBCOL plugin on ImageJ (n=15 for each marker and time point from three independent experiments). Error bars represent SEM. (**D**) HeLa monolayers from (B) were harvested by washing in EDTA/PBS, and the cells in suspension stained for either transferrin receptor with OKT9 antibodies or mouse monoclonal anti-human APP antibodies. Incubation with Pitstop 2 increased the level of transferrin receptor (TfR) on the PM whereas very little APP is detected at the PM.

Figure 3: Arf1 and Arf4 depletion does not affect APP localisation
HeLa cells stably expressing APP_{695wt} or HeLa cells were transfected with either control siRNA, Arf1 and/or Arf4 siRNAs for 72 h. (**A&B**) Cells were lysed in SDS-PAGE reducing buffer and cell extracts were subjected to SDS-PAGE on 4-12% gradient polyacrylamide gel. Proteins were transferred to a PVDF membrane and probed with (**A**) mouse polyclonal anti-Arf1 antibody and mouse anti-±-tubulin antibody and (**B**) mouse anti-AP1³ antibody, mouse polyclonal anti-Arf1 antibody, rabbit anti-Arf4 antibody and mouse anti-±-tubulin antibody using a chemiluminescence detection system. (**C**) HeLa cells stably expressing APP_{695wt} monolayers were fixed, permeabilized and blocked before staining with mouse monoclonal anti-human APP antibodies (red) and rabbit polyclonal antibodies to GCC88 (green). Higher magnification of the merged images is also shown. Bars represent 10 µm. (**D**) The percentage of APP at the TGN was calculated from the percentage of total APP pixels that overlapped with GCC88. All calculations were performed using the OBCOL plugin on ImageJ (n=15 for each marker and condition from three independent experiments). Error bars represent SEM. (**E**) HeLa cells monolayers were fixed, permeabilized and blocked before staining with mouse anti-AP1³ antibody (red) and rabbit polyclonal antibodies to GCC88 (green).

Figure 4: Arl5b depletion results in APP accumulation in the TGN
(**A-B**) HeLa cells stably expressing Arl5b(Q70L)-GFP were transfected with either control siRNA or Arl5b siRNAs for 72 h. (**A**) Cells were lysed in SDS-PAGE reducing buffer and cell extracts were subjected to SDS-PAGE on 4-12% gradient polyacrylamide gel. Proteins were transferred to a PVDF membrane and probed with rabbit anti-GFP antibody, and mouse anti-±-tubulin antibody, using a chemiluminescence detection system. (**B**) Monolayers were fixed, permeabilized, stained with DAPI (blue) and Arl5b-GFP detected by GFP fluorescence. (**C**) HeLa cells stably expressing APP_{695} were transfected with either control siRNA or Arl5b siRNAs for 72 h. Monolayers were fixed and permeabilized and stained with mouse monoclonal anti-human APP antibodies (red) and rabbit antibodies to GCC88 (green). Higher magnification of the merged images is also shown. (**D**) The percentage of APP at the TGN was calculated from the percentage of total APP pixels that overlapped with GCC88. Calculation was performed using the OBCOL plugin on ImageJ (n=15 for each marker and condition from three independent experiments). Error bars represent SEM. *** $p<0.001$, ** $p<0.01$. (**E**) Expression of an siRNA-1 resistant Arl5b-GFP construct (Arl5b-Rescue-GFP) in Arl5b-1 siRNA treated HeLa cells stably expressing APP_{695wt}. Cell expressing the Arl5b-GFP rescue construct is outlined. Bars represent 10 µm.

Figure 5: Arl5b depletion results in CD8/APP accumulation in the TGN

(**A**) HeLa cells were transfected with either control siRNA or Arl5b siRNAs for 48 h and then transfected with CD8/APP constructs for 24 h. After 24 h, monolayers were fixed and permeabilised and then stained with mouse polyclonal anti-CD8 antibodies (red) and GCC88 (green). Higher magnification of the merge images are also shown. Bars represent 10 µm. (**B**) The percentage of CD8-APP at the TGN was calculated from the percentage of total CD8/APP pixels that overlapped with GCC88. All calculations were performed using the OBCOL plugin on ImageJ (n=15 for each marker and condition from three independent experiments). Error bars represent SEM. *** $p<0.001$, ** $p<0.01$.

Figure 6: AP4µ depletion results in APP accumulation in the TGN

(A) Quantitative PCR (qRT-PCR) analysis of AP4µ depletion. Total RNA was isolated from HeLa cells transfected with either control siRNA or AP4µ siRNAs for 72 h. Total RNA was converted to cDNA to setup singleplex reactions in quadruplicate for AP4 with the internal endogenous reference gene, GAPDH. qRT-PCR was performed using the comparative DeltaDelta CT method. Relative quantification of mRNA levels was achieved using control siRNA as the normaliser. Data was pooled from three independent experiments and analysed by a paired, two-tailed student *t*-test. (**B**) HeLa cells stably expressing APP_{695wt} were transfected with either control siRNA or AP4µ siRNAs for 72 h. Monolayers were fixed and permeabilized and stained with mouse monoclonal anti-human APP antibodies (red) and GCC88 (green). Higher magnification of the merges images is also shown. Bars represent 10 µm. (**C**) The percentage of APP at the TGN was calculated from the percentage of total APP pixels that overlapped with GCC88 using the OBCOL plugin on ImageJ. Data is pooled from three independent experiments and expressed as the mean +/- SEM (n=15) and analysed by an unpaired, two-tailed student *t*-test *** $p<0.001$.

Figure 7: Arl5b and AP4µ depletion alters APP distribution in the entire cell population

(**A-D**) HeLa cells stably expressing APP_{695wt} were transfected with either control siRNA, Arl5b siRNA or AP4µ siRNAs for 72 h. Cells were lifted with 5 mM EDTA/PBS and cells in suspension then fixed and permeabilized and stained with mouse anti-APP (A, B) or rabbit GRASP65 antibodies (**C, D**). Stained cells were analysed by flow cytometry where 10,000 events were collected per sample. Histograms of the fluorescent pulse width of APP (**A**) and GRASP65 (**C**) are shown. A rightward shift in the histogram in A represents an increased fluorescent pulse width while a leftward shift represents a decreased pulse width. Histograms were overlaid using Flowjo. (**B, D)** Bar graph showing the statistically analysis of the median fluorescent pulse width of APP and GRASP65 under control and Arl5b or AP4µ depleted conditions. Data is pooled from three independent experiments. Error bars represent SEM. *** $p<0.001$.

Figure 8: AP4 interacts with Arl5b (Q70L)

(**A**) HeLa cells stably expressing constitutive active Arl5b (Q70L)-GFP or HeLa cells transiently transfected with a GFP vector were lysed and extracts immunoprecipitated using monoclonal antibodies to the GFP tag. Immunoprecipitated complexes were subjected to SDS-PAGE on 4–12% gradient polyacrylamide gel. Whole cell lysates (input) were included as loading controls. Proteins were transferred to a PVDF membrane and probed for AP4µ, AP4ε, Arf1, $AP1^3$ and GFP as indicated. (**B**) HeLa cell monolayers were transfected with Arl5b-GFP (Q70L) for 24 h, fixed and permeabilized, and staining with either mouse anti-AP4 8 GCC88 antibodies or rabbit (**C**) arfHeLa cell monolayers were transfected with either control siRNA, Arf1 siRNA or Arl5b siRNA for 72 h. In addition, cells transfected with Arl5b siRNA were also co-transfected 48 h later with an siRNA resistant Arl5b-GFP construct as indicated for a further 24 h. Monolayers were fixed and permeabilized and stained with mouse anti-AP4ε antibodies (red) and rabbit anti-GCC88 antibodies (green). (**D**) Bar graphs showing AP4ε fluorescence intensity in the Golgi region as a ratio of total cytoplasmic fluorescence for each condition, as described under Methods. Data was pooled from three independent experiments and is expressed as the mean +/- SEM (n=15). *** $p<0.001$

Figure 9: Arl5b and AP4µ depletion results in AP4 dispersal in the cytoplasm

(**A-F**) HeLa cells were transfected with either control siRNA, Arl5b siRNA or AP4µ siRNAs for 72 h. Monolayers were lifted by incubation with 5 mM EDTA/PBS and cells in suspension fixed and permeabilized and staining with either mouse anti-AP4ε, antibodies, mouse anti-$AP1^3$ antibodies or rabbit anti-GRASP65 antibodies. Stained cells were analysed by flow cytometry and 10,000 events were collected per sample. Histograms of the fluorescent pulse width of (**A**) AP4ε, (**C**) $AP1^3$ and (**E**) GRASP65 of siRNA treated samples are shown. A rightward shift in the histogram represents an increased pulse width while a leftward shift represents a decreased pulse width. Histograms were overlaid using Flowjo. (**B, D & F)** Bar graphs showing the statistical analysis of the median pulse width of the (**B**) AP4ε, (**D**) $AP1^3$ or (**F**) GRASP65 in control, Arl5b or AP4µ depleted conditions. Data was pooled from three independent experiments. Data is expressed as the mean +/- SEM. *** $p<0.001$, ** $p<0.01$.

Figure 10: APP processing and A^2 production is increased in Arl5b and AP4µ depletion cells

(A) HeLa cells stably expressing APP_{695wt} were transfected with either control siRNA, Arl5b siRNA or AP4μ siRNA for 72 h then conditioned media containing collected over 16 h and analysed for the presence of secreted A² using a sandwich ELISA specific for A^2_{40}. The levels of A^2_{40} for each sample were normalized against total cell protein. Data was pooled from 4 independent experiments and expressed as the mean +/- SEM. *** $p<0.001$ (**B**) Conditioned media from each sample was subjected to SDS-PAGE, transferred onto membrane and probed with mouse W02 antibody to detect sAPP±. (**C**) Bar graph of the intensity of the sAPP± bands from 4 independent experiments. The levels of the sAPP± in these experiments were normalised for against total cell protein levels. Densitometry of bands was carried out using ImageJ. Data is expressed as the mean +/- SEM. (**D**) HeLa cells stably expressing APP_{695wt} were transfected with either control siRNA, Arl5b siRNA or AP4ε siRNA for 72 h and then treated with 250 nM ³-secretase inhibitor DAPT or DMSO carrier control for 16 h and then cells were lyzed. Cell lysates (20 μg/sample) were subjected to SDS-PAGE, transferred onto either PVDF membrane and probed with antibodies to detect AP4ε or α-tubulin or nitrocellulose membrane and probed with mouse W02 antibody to detect β-CTF. (**E**) Bar graphs showing fold change of β-CTF levels from each condition from 4 independent experiments. Data for the AP4ε siRNA and Arl5b siRNA are represented as fold changes compared to control siRNA, mean +/- SEM.

Figure 11: Model of anterograde transport of newly synthesised APP and BACE1
Both APP and BACE1 are synthesised as membrane proteins in the ER and subsequently are transported to the Golgi. At the TGN the two membrane cargoes follow distinct pathways to the plasma membrane, APP is transported by an Arl5b and AP4 dependent pathway to the early endosome then late endosomes whereas BACE1 is proposed to be transported either directly to the plasma membrane or indirectly via recycling endosomes.

Supplementary Figure legends

Figure S1: Steady state distribution of APP in HeLa cells
(**A**) Monolayers of HeLa cells stably expressing APP_{695wt} were fixed and permeabilized and stained with monoclonal mouse anti-human APP antibodies (red) and intracellular markers to either the trans Golgi network (TGN) (GCC88), early endosomes (EEA1), late endosomes (Rab7) and recycling endosomes (Rab11) (green). Bar represents 10 μm. (**B**) Analysis of cell surface APP by flow cytometry. Monolayers of either wild-type HeLa cells or HeLa cells stably expressing $APP_{695wt,}$ as indicated, were harvested by washing in EDTA/PBS, and cells in suspension stained with monoclonal mouse anti-human APP antibodies and Alexa488 -conjugated anti-mouse IgG, then fixed and analysed by flow cytometry. (**C**) Monolayers of HeLa cells stably expressing APP_{695wt} were fixed and permeabilized and stained with monoclonal mouse anti-human APP antibodies (N-term APP) (red) (Clone NAB228) and rabbit antibodies to APP which recognise the C-terminal tail (C-term APP) (green). (**D**) Wild type HeLa cells and HeLa cells stably expressing APP_{695wt} or HeLa cells were lysed in SDS-PAGE reducing buffer and cell extracts were subjected to SDS-PAGE on 4-12% gradient polyacrylamide gel. Proteins were transferred to a PVDF membrane and probed with monoclonal mouse anti-human APP antibodies (Clone WO2) and mouse anti-±-tubulin antibody.

Figure S2: APP does not traffic to the recycling endosomes
HeLa cells stably expressing APP_{695wt} were treated with 50 μg/mL cycloheximide (CHX) for 4 h. Cell monolayers were then washed twice with PBS and protein synthesis resumed by incubating cells in C-DMEM at 37 ºC. Cells were fixed at different time points for up to 7 h after CHX washout as indicated. Monolayers were permeabilized and stained with mouse monoclonal anti-human APP antibodies (red) and rabbit polyclonal antibodies to Rab11 (green) and DAPI (blue) at different time points. Bar represents 10 μm.

Figure S3: Increase in cell surface expression of transferrin receptor following Pitstop 2 treatment
HeLa monolayers were incubated in serum-free DMEM containing 30 μM Pitstop 2 or 0.1% DMSO (carrier control) at 37 ˚C for 45 min. Monolayers were harvested by washing in EDTA/PBS, and cells in suspension stained for cell surface transferrin receptor (TfR) with OKT9 antibodies and Alexa488-conjugated anti mouse IgG, fixed in 4% PFA and analysed by flow cytometry. A total of 10 000 events were collected per sample. Histograms were overlaid using Flowjo.

Figure S4
HeLa cells stably expressing APP_{695wt} were transfected with either control siRNA, Arl5b siRNA or AP4ε siRNAs for 72 h. Monolayers were fixed, permeabilzsed and blocked before staining with mouse monoclonal anti-human APP antibodies (N-

term APP) (red) (Clone NAB228) and rabbit antibodies to APP which recognise the C-terminal tail (C-term APP) (green). Bar represents 10 μm.

Figure S5: Arl5b depletion does not alter BACE1 distribution

(**A**) Wild-type HeLa cells were transfected with either control siRNA or Arl5b siRNA for 48 h and then transfected with a BACE1 construct for 24 h. Monolayers were then fixed, permeabilised and stained with rabbit polyclonal anti-BACE1 antibodies (red) and mouse polyclonal antibodies to golgin97 (green). Higher magnification of the merged images are also shown. Bars represent 10 μm. (**B**) The percentage of BACE1 at the TGN was calculated from the percentage of total BACE1 pixels that overlapped with golgin97. All calculations were performed using the OBCOL plugin. Data was pooled from three independent experiments and is expressed as the mean +/- SEM (n=15 for each treatment).

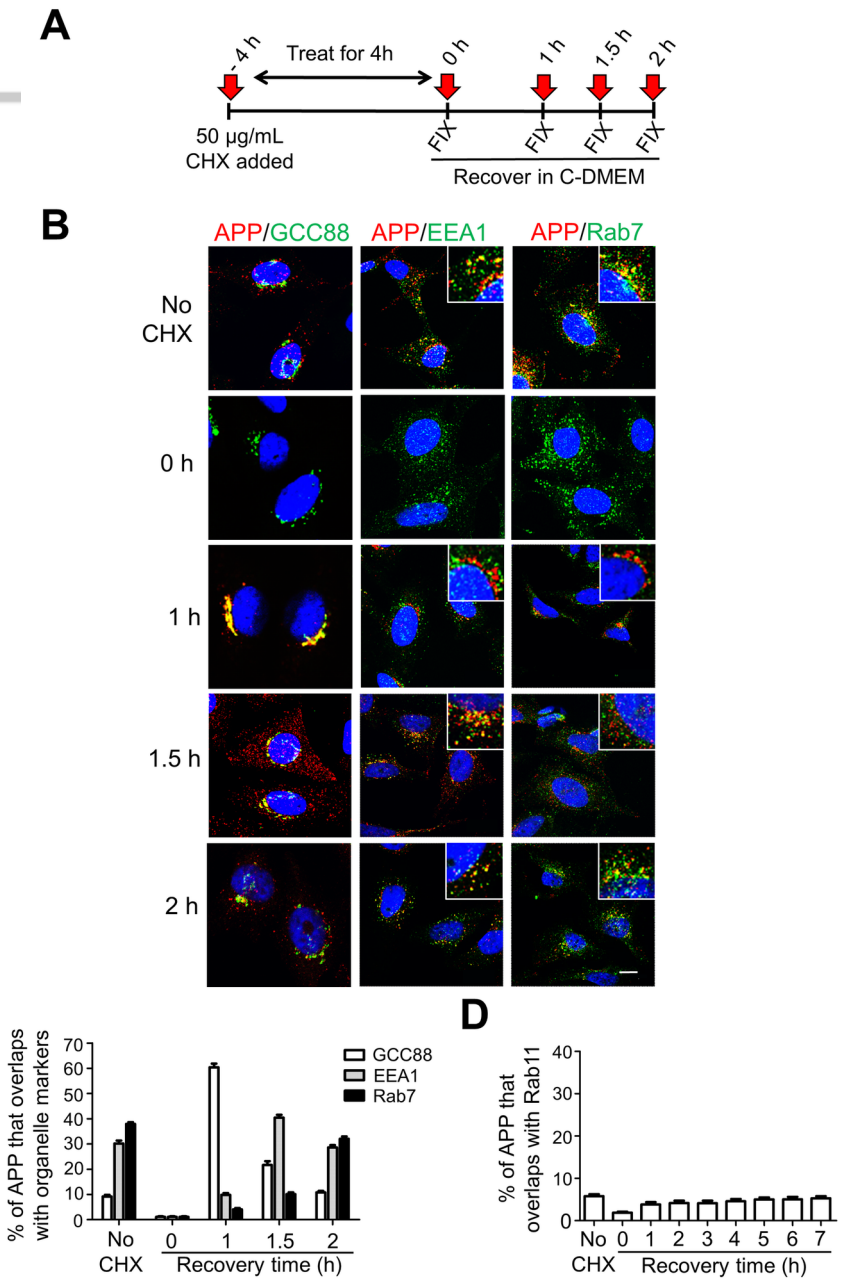

Figure 1.TIF

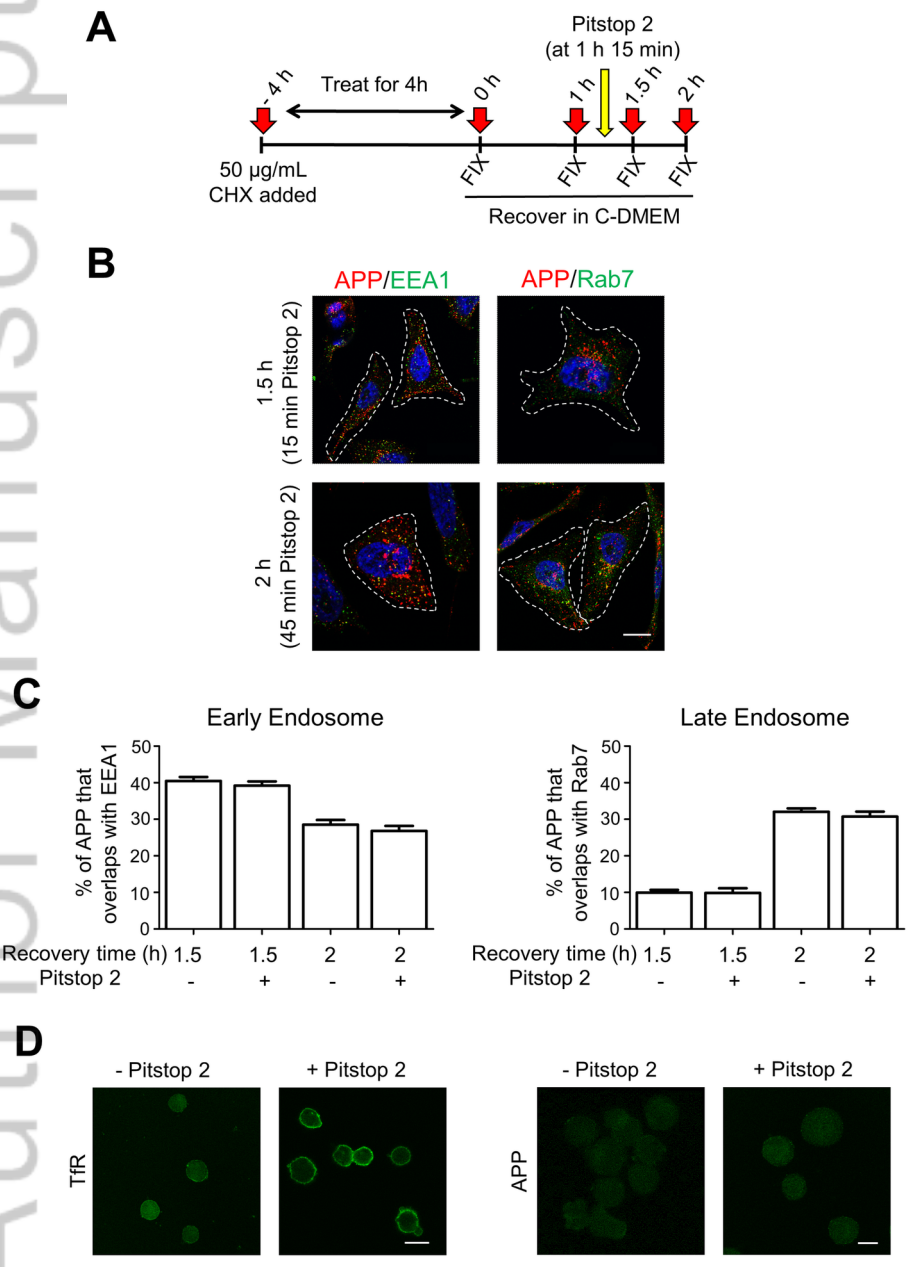

Figure 2.TIF

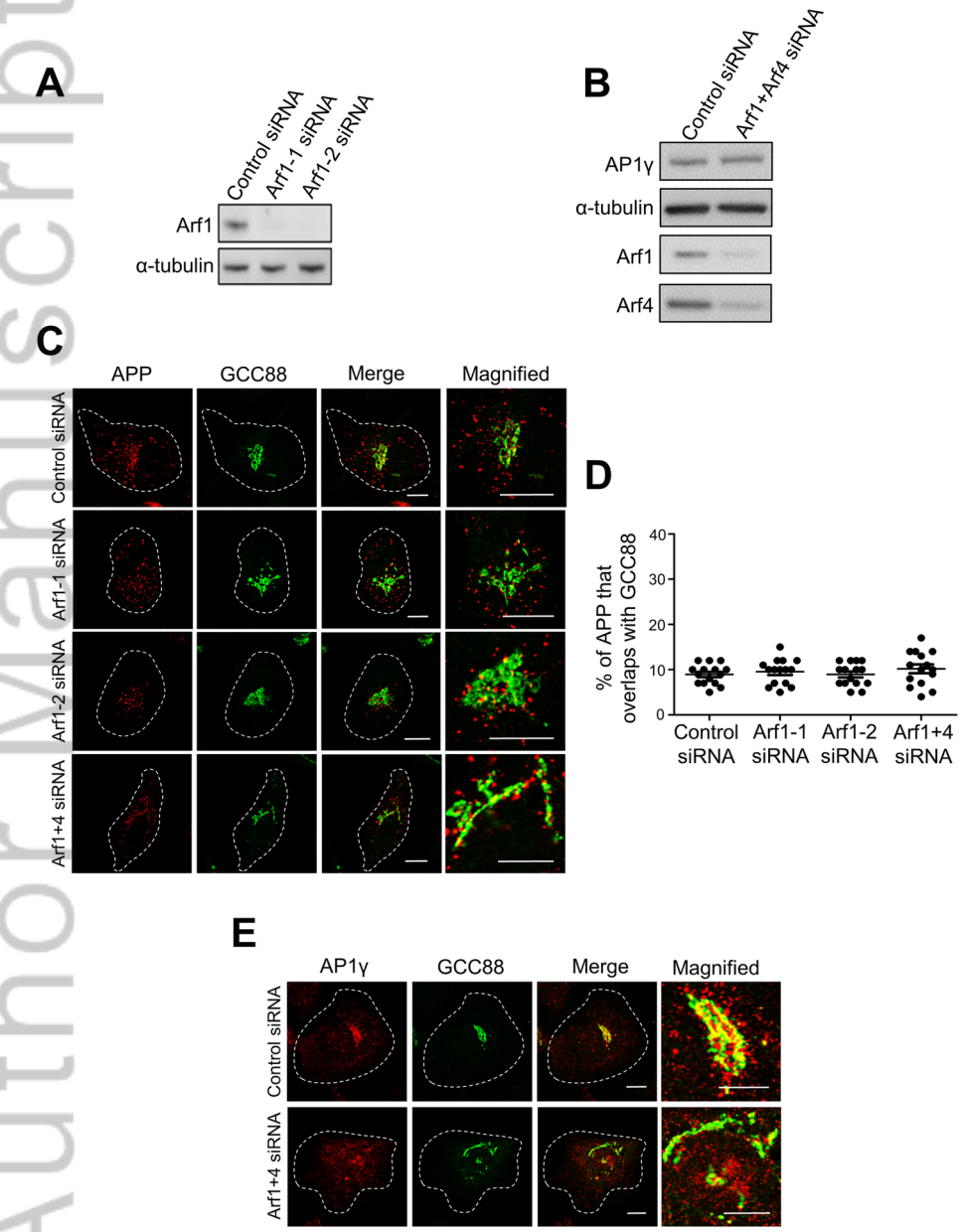

Figure 3.tif

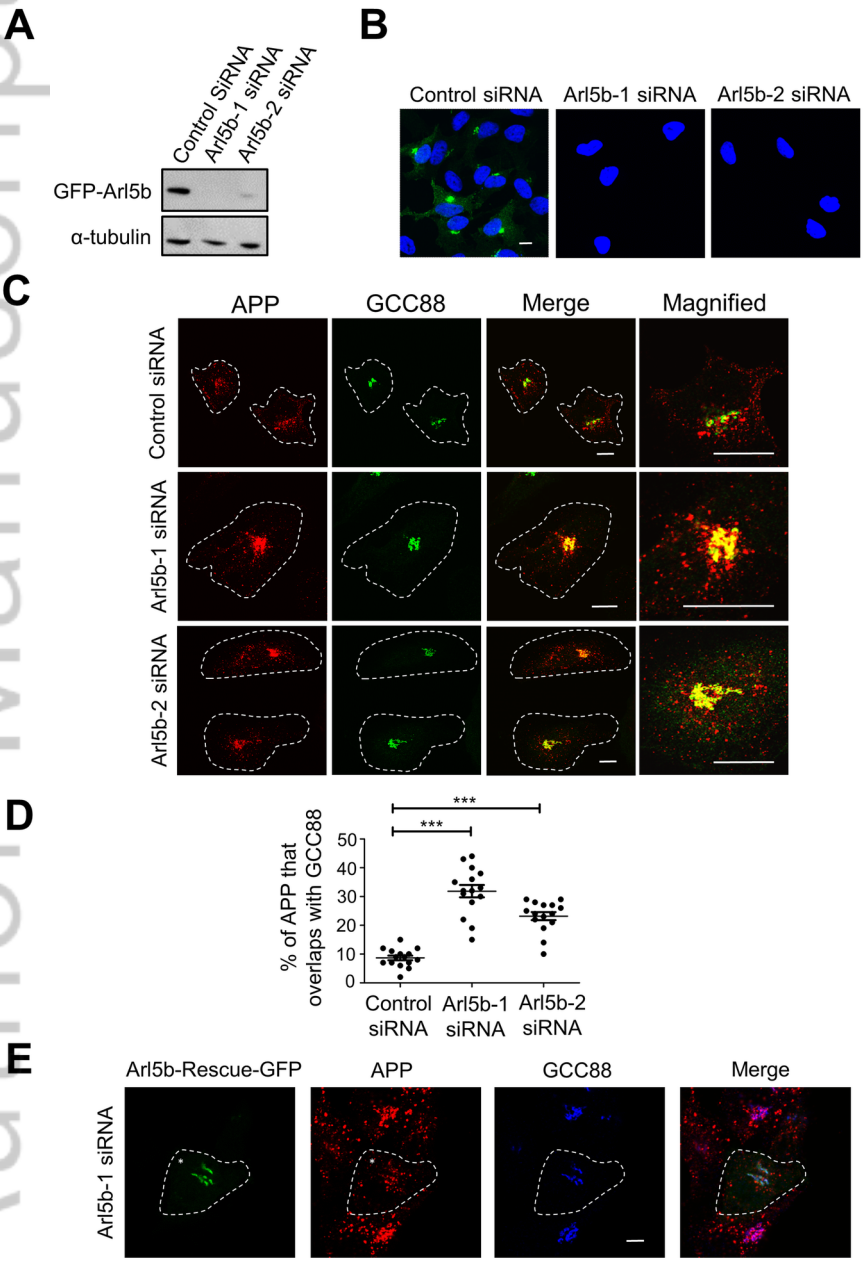

Figure 4.TIF

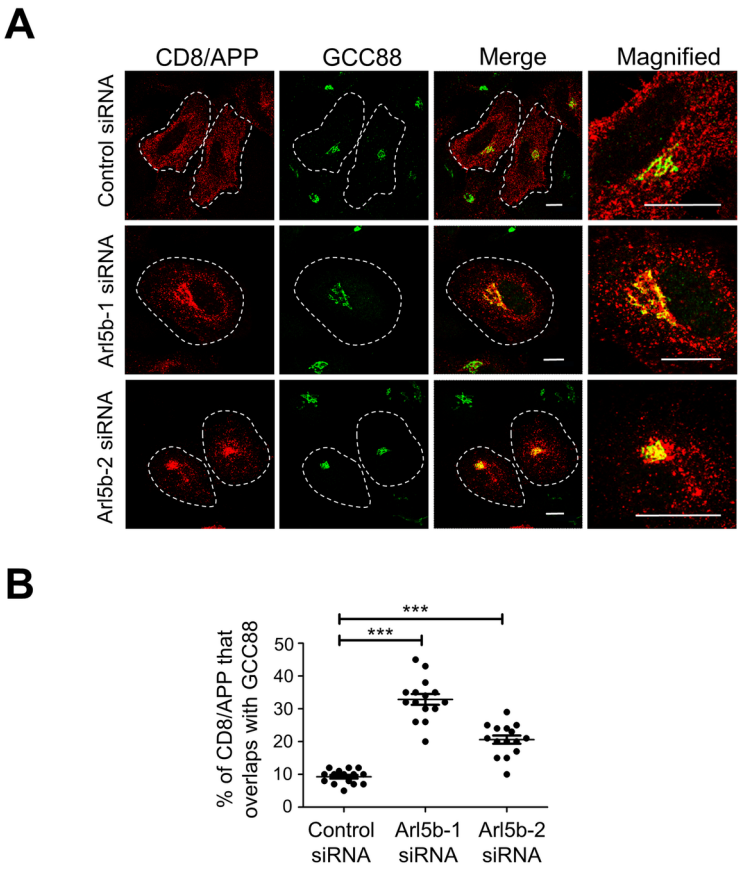

Figure 5.TIF

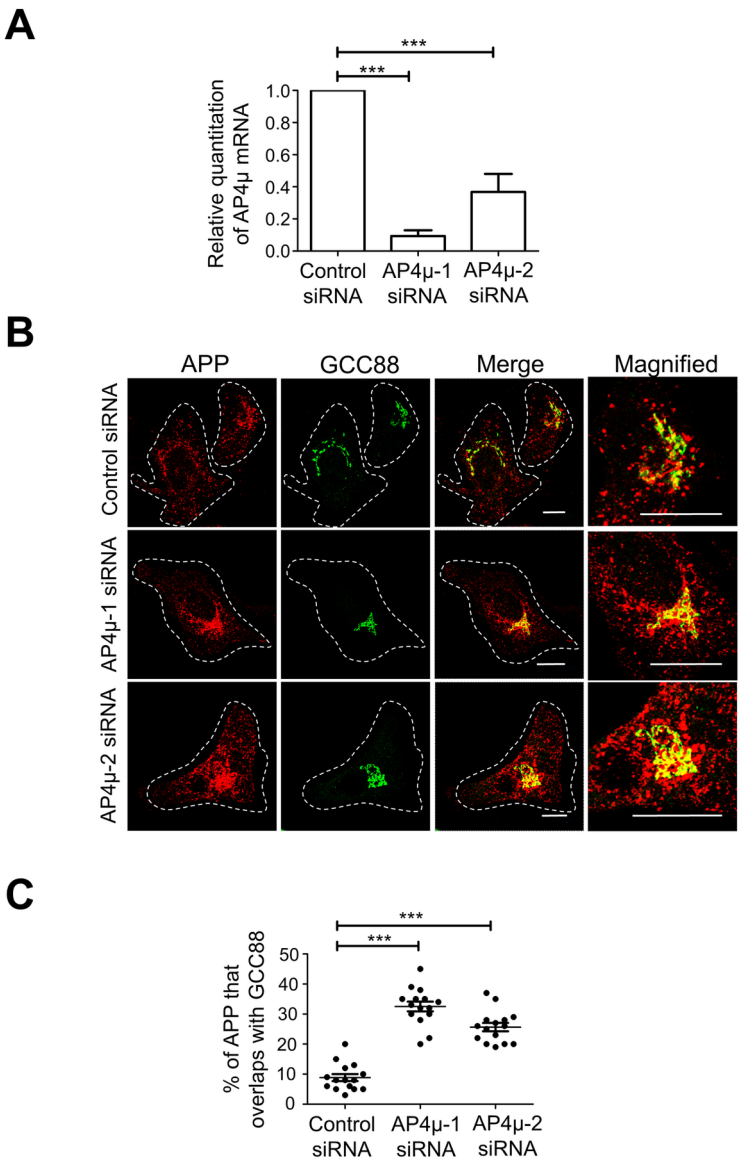

Figure 6.TIF

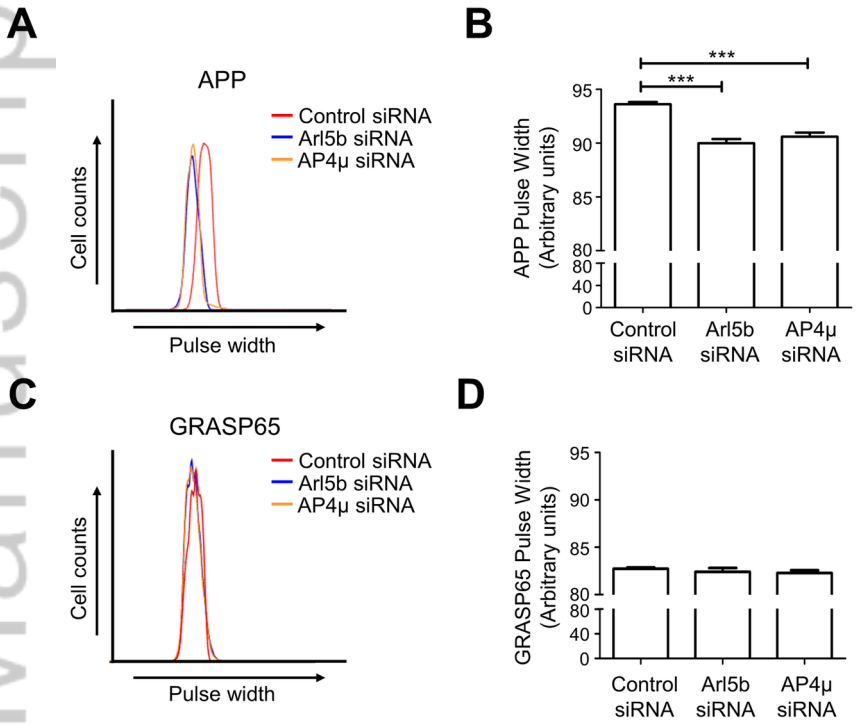

Figure 7.TIF

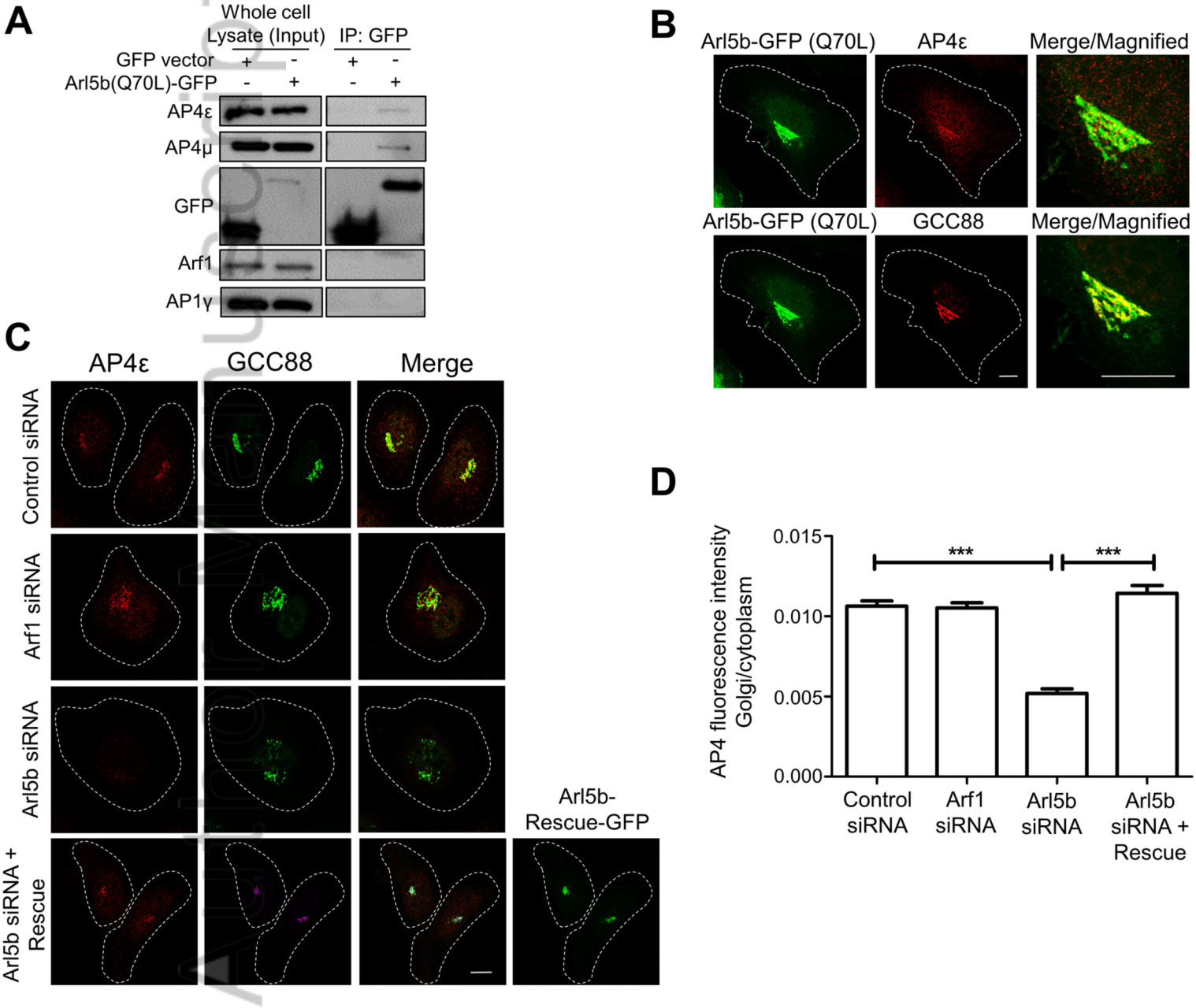

Figure 8.tif

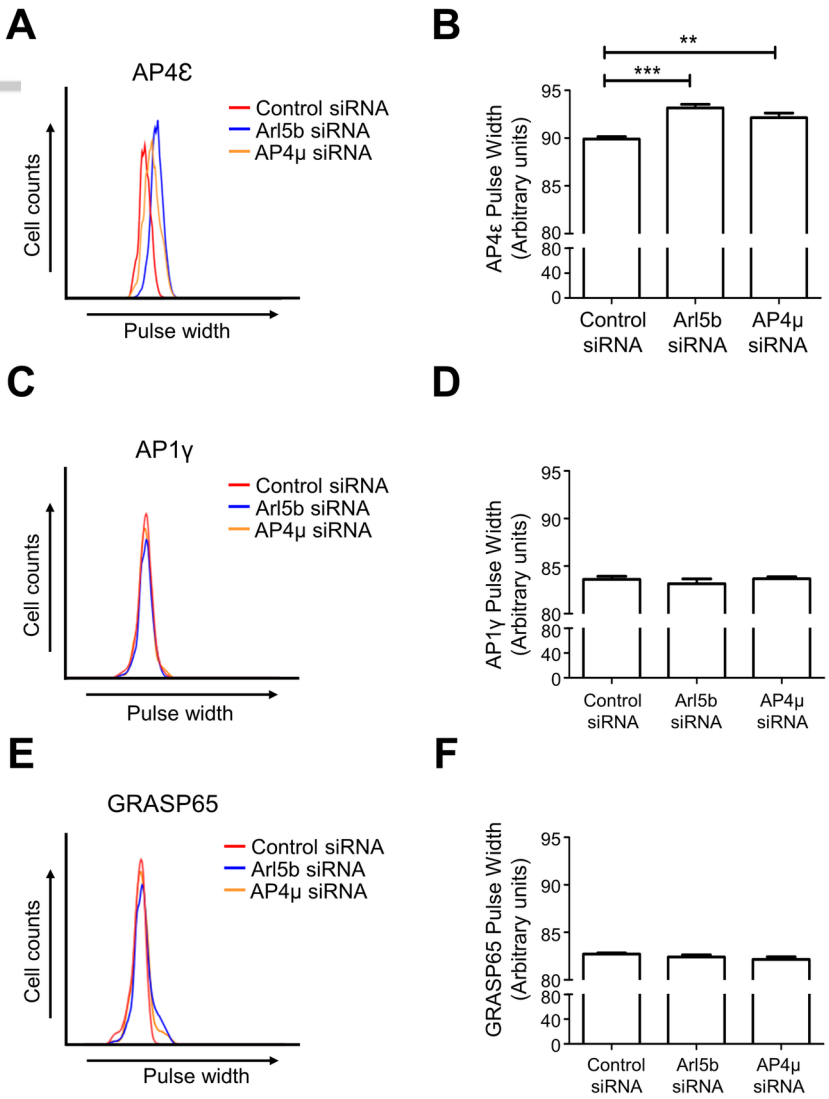

Figure 9.TIF

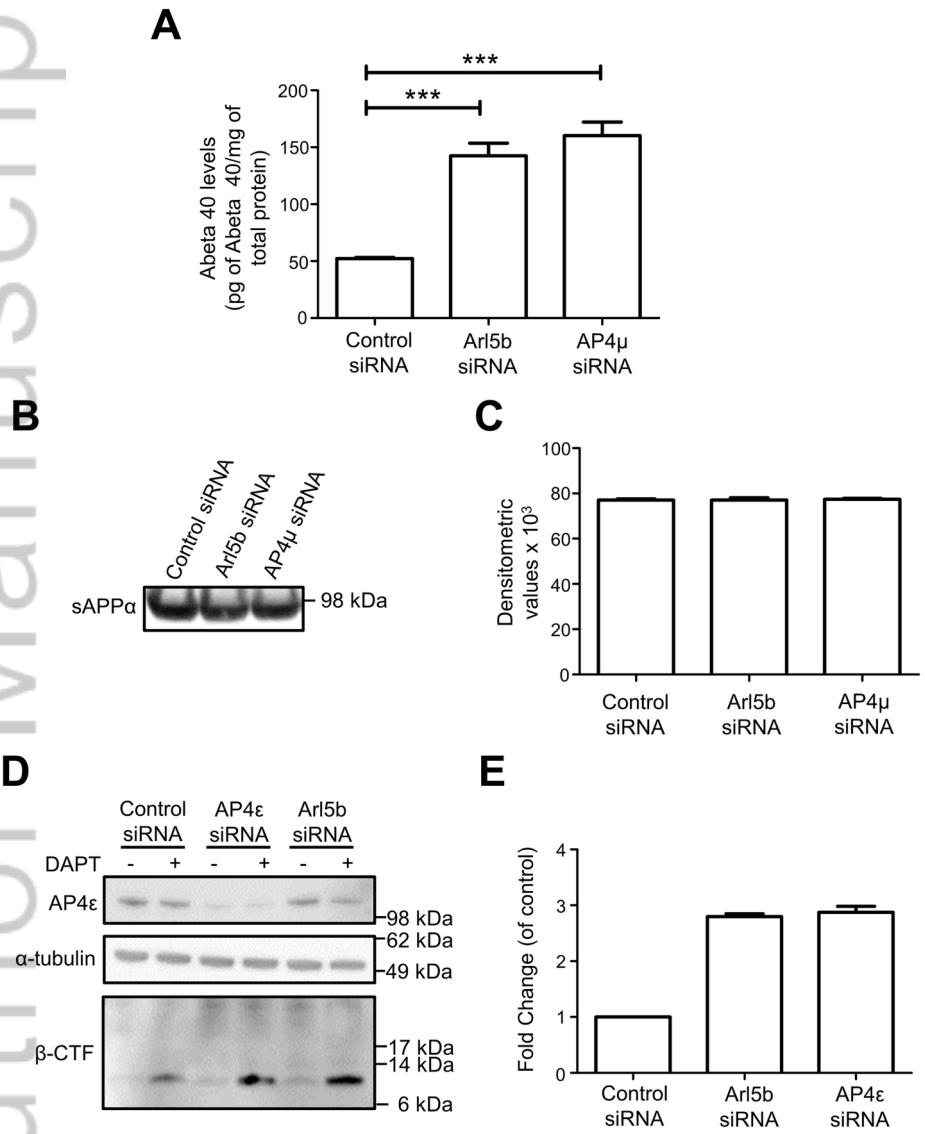

Figure 10.TIF

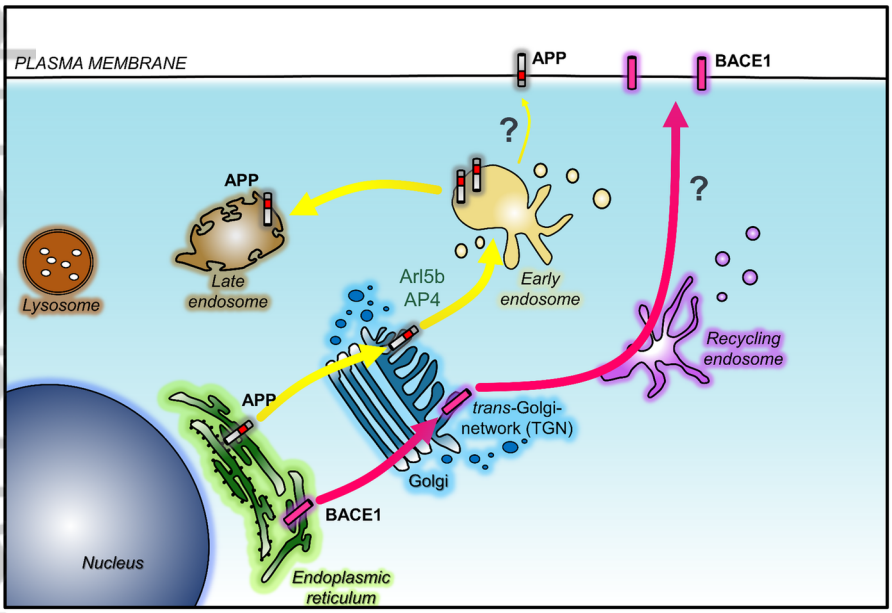

Figure 11.TIF

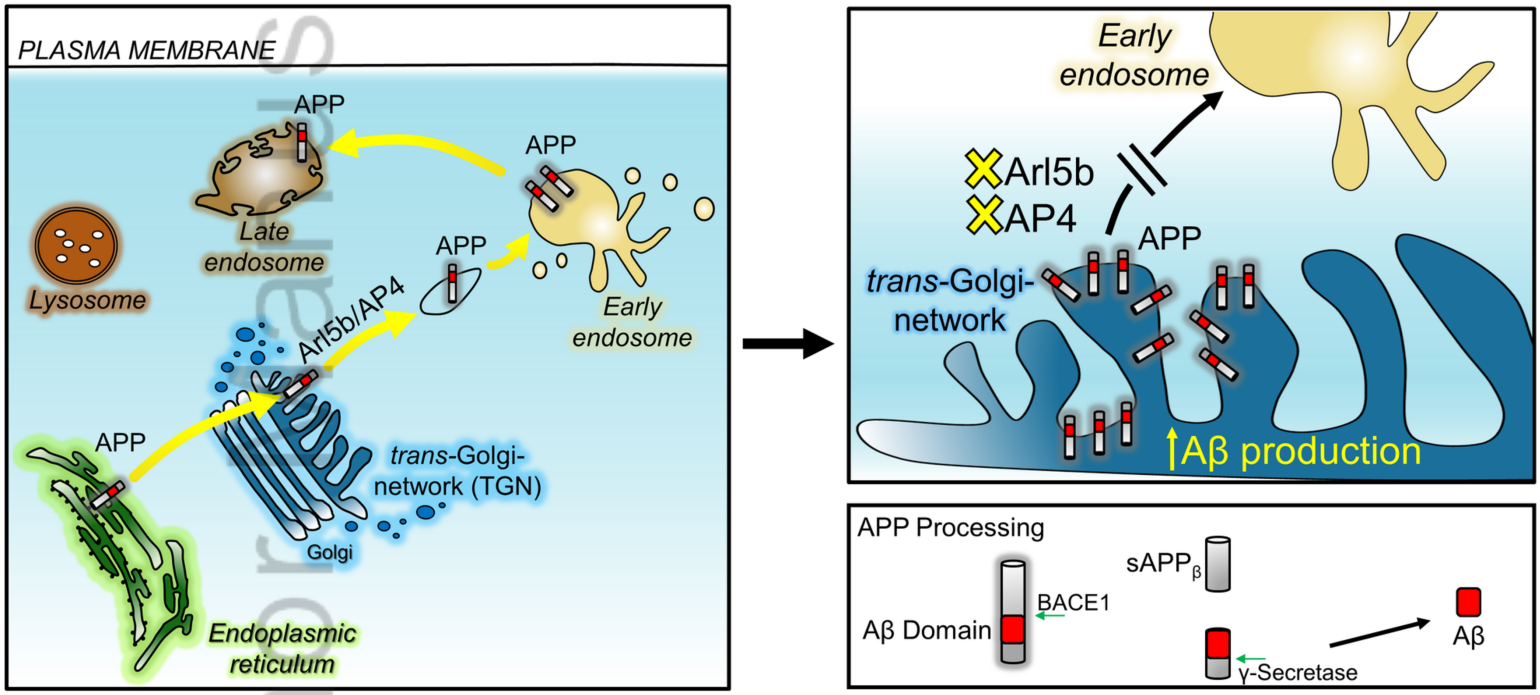

tra_12465_AbstractFigure.tiff